First principle investigation of CO_2 conversion on Pd−polyaniline interface

A Thesis

submitted to

Indian Institute of Science Education and Research Pune

in partial fulfillment of the requirements for the

BS-MS Dual Degree Programme

by

Amit Sahu

IISER PUNE

Indian Institute of Science Education and Research Pune

Dr. Homi Bhabha Road,

Pashan, Pune 411008, INDIA.

April, 2018

Supervisor: Dr. Prasenjit Ghosh

© Amit Sahu 2018

Certificate

This is to certify that this dissertation entitled First principle investigation of CO_2 conversion on Pd−polyaniline interface towards the partial fulfilment of the BS-MS dual degree programme at the Indian Institute of Science Education and Research, Pune represents work carried out by Amit Sahu at Indian Institute of Science Education and Research under the supervision of Dr. Prasenjit Ghosh, Associate Professor, Department of Physics and Chemistry , during the academic year 2017-2018.

Prasenjit Ghosh

Dr. Prasenjit Ghosh

Committee:

Dr. Prasenjit Ghosh

Dr. Mukul Kabir

This thesis is dedicated to the greatest influence of my life my lovely mother.

Declaration

I hereby declare that the matter embodied in the report entitled First principle investigation of CO_2 conversion on Pd−polyaniline interface are the results of the work carried out by me at the Department of Physics and Chemistry, Indian Institute of Science Education and Research, Pune, under the supervision of Dr. Prasenjit Ghosh and the same has not been submitted elsewhere for any other degree.

Amit Sahu

Acknowledgments

Abstract

Electrocatalytic reduction of CO_2 (ERC) in the presence of aqueous electrolyte has attracted huge attention of the scientific community due to its ability to utilize CO_2 and recycle it to form renewable energy resources. The challenges behind its commercialization are: (a) poor selectivity of the catalyst towards CO_2 reduction, (b) requirement of high overpotential for CO_2 activation and (c) bad product selectivity of the catalyst. Recently, Weiran Zheng *et. al.* had proposed the use of Pd-Polyaniline (Pd-PANI) interface as a potential catalyst for ERC with very high selectivity towards the formation of formic acid. However, the mechanistic details are not yet clearly understood. Herein, with the help of density functional theory (DFT) calculation, we investigate the detailed mechanism of CO_2 reduction by taking into account all possible reactions pathways on PANI and Pd-PANI. We have included the implicit solvent model to enhance the correlation of our studies with the experiment. From the studies, we observe that the solvent stabilizes the intermediates via non-covalent interactions. Our calculations suggest the activation of CO_2 is robust on Pd-PANI as compared to Pd or PANI. Furthermore, ERC on PANI is selective towards *COOH (carboxyl) intermediate rather than *OCHO (formate) intermediate, while the reverse is observed on Pd-PANI. There was hardly any methanol formation on PANI whereas methanol formation occurred at a high energy cost on Pd-PANI. From our calculations, we were able to explain the reasons behind more selectivity towards formic acid rather than methanol formation and also trace amount of CO formation at high overpotential (-1.1 eV) on Pd-PANI, as observed in the experimental studies.

Contents

List of Figures

List of Tables

Chapter 1

Introduction

I N the past century due to industrial revolution there has been a humongous amount of increase in industrial activities that has spoiled the balance of CO_2 in atmosphere[1]. Everlasting increase in concentration of CO_2 in the atmosphere causes greenhouse effect resulting in global warming in the atmosphere which is a major issue of Earth's environment[2, 3]. To maintain the balance either we have to reduce the production of CO_2 or recycle this molecule to some useful ones[1]. CO_2 is highly stable and chemically inert. Therefore its quite difficult to break it and convert it to any other molecule under ambient conditions[4]. Reduction of CO_2 could be a promising approach for converting it to usable fuels[5]. If it is possible to reduce the CO_2 in commercial scale at low cost it will be a huge reward for the mankind because it can significantly reduce the CO_2 in atmosphere. Some useful products such as formic acid and methanol based carbon neutral cycle has been shown in figure:1.1.

There are many different methods from which CO_2 can be reduced and converted into useful products. However the cost we need to pay to convert CO_2 is very high. Hence it's large scale conversion is still a challenge. Many attempts had been made to improve CO_2 conversion at a reduced energy cost. Possible ways of CO_2 conversion have been listed in table:1.1. In radiochemical method it requires γ radiation which demand very high energy to generate it. Chemical reduction by metals through the thermocatalytic method involve very high temperatures. In photocatalytic process the conversion efficiency (around $< 2\%$)is very far from the desirable level required for industry[6]. Electrocatalytic reduction of CO_2 (ERC) also require a high overpotential (1 eV). Since this thesis deals with ERC, we describe it in more details in the next section.
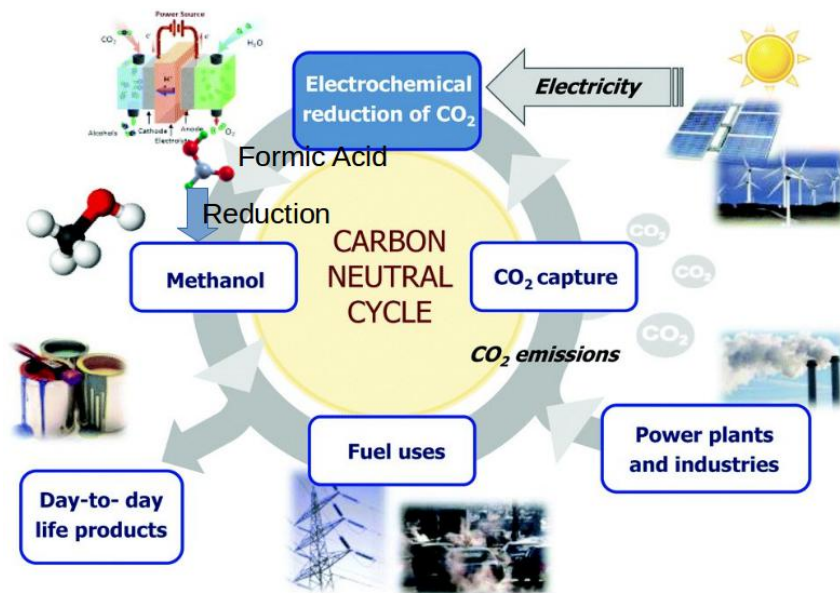
Figure 1.1: Methanol and formic acid based CO$_2$ cycle model adapted from [1]

Method	Examples
Radiochemical	$CO_2 \xrightarrow{\gamma\ radiation} HCOOH_H CHO$
Chemical reduction by metal	$2\,Mg + CO_2 \xrightarrow{high\ T} 2\,MgO + C$ $Sn + 2CO2 \rightarrow SnO_2 + 2\,CO$ $2Na + 2CO2 \rightarrow Na_2C_2O_4$
Thermo-catalytic	$CO_2 \xrightarrow{Ce^{4+},T>900} CO + \frac{1}{2}O_2$
Photo-catalytic	$CO_2 \xrightarrow{h\nu} CO + HCHO + HCOOH$
Electro-catalytic	$CO_2 + ne^- + nH^+ \xrightarrow{eV} COHCOOHCH_3OH\ \cdot\cdot$

Table 1.1: Different possible methods for reducing CO$_2$ and corresponding examples.

1.1 Electrocatalytic reduction of CO$_2$

From past decade onwards ERC has gained huge attention from scientific community due to controllability of process by electrode potential and temperature and recoverability of supported electrolyte[6]. ERC can proceed through multi-electron reduction pathways and produce many diverse products ranging from hydrocarbons (C$_2$H$_2$, CH$_4$), liquid fuels (MeOH, HCOOH) to CO. However, many open challenges remain such as slow kinetics of CO$_2$ reduction and low efficiency even at high overpotential. The equilibrium potential of CO$_2$ reduction at a pH of 7.0 and at room temperature for different products along with hydrogen

evolution reaction (HER) has been given below[4].

$$CO_2 + 6\,H_2O + 8\,e^- \xrightleftharpoons{-0.25V} CH_4 + 8\,OH_{(aq)}^- \tag{1.1}$$

$$3\,CO_2 + 13\,H_2O + 18\,e^- \xrightleftharpoons{-0.32V} C_3H_7OH + 18\,OH_{(aq)}^- \tag{1.2}$$

$$2\,CO_2 + 9\,H_2O + 12\,e^- \xrightleftharpoons{-0.33V} C_2H_5OH + 12\,OH_{(aq)}^- \tag{1.3}$$

$$2\,CO_2 + 8\,H_2O + 12\,e^- \xrightleftharpoons{-0.34V} C_2H_4 + 12\,OH_{(aq)}^- \tag{1.4}$$

$$CO_2 + H_2O + 2\,e^- \xrightleftharpoons{-0.43V} HCOO^- + OH_{(aq)}^- \tag{1.5}$$

$$CO_2 + H_2O + 2\,e^- \xrightleftharpoons{-0.52V} CO + 2\,OH_{(aq)}^- \tag{1.6}$$

$$2\,H_2O + 2\,e^- \xrightleftharpoons{-0.41V} H_2 + 2\,OH_{(aq)}^- \tag{1.7}$$
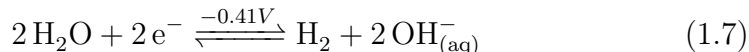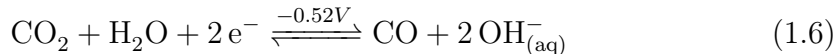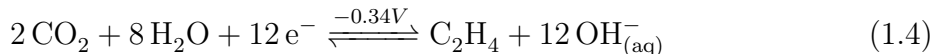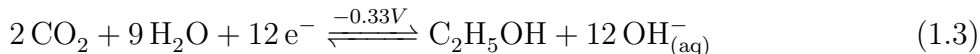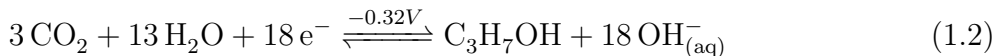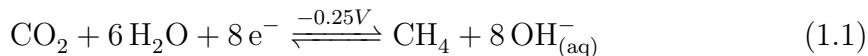
From these equations we can see that the equilibrium potential of CO_2 reduction is not very different from that of electrocatalytic reduction of water. So there will be a chance of reducing water instead of CO_2. Moreover, the equilibrium potential is not very different for different products. So there are two major problems which need to be addressed: one is to reduce the probability of water reduction instead CO_2, and another one is selectivity towards the desired product due to similar equilibrium potential[4]. However, the present day commercialized catalysts are neither active enough nor highly selective.

So now the challenge is to improve the selectivity of the catalyst towards CO_2 reduction instead of water and product formation. Furthermore, even though the equilibrium potential of CO_2 is low, ERC does not occur easily due to the high overpotential required for the first electron transfer, which is the rate determining step of ERC ($CO_2 + e^- \longrightarrow CO_2^{\cdot-}$)[4]. Existence of other pathways like formation of H_2 through hydrogen evolution reaction (HER) and CO make it more difficult. The types of species formed in the reaction will highly depend on the selectivity of the catalyst and the applied overpotential[6]. Production of formic acid and methanol is highly desirable products. Formic acid is used as an important chemical in food, pharmaceutical and textile industry due to its strong reducing properties and highly acidic nature. Formic acid can also be used in fuel cell[7]. Methanol (MeOH) can be used as a fuel, for hydrogen storage and as a raw-material for olefin synthesis[8].

Recently Weiran Zheng *et al.* have shown that transition metal-polyaniline (M-PANI) interface could be an efficient catalyst for electro-reduction of CO_2 to formic acid and methanol. ECR in aqueous electrolyte, with Pd as a catalyst promotes the formation of H_2 due to reduction of water. When PANI is used as a catalyst it reduces CO_2 but the efficiency is very low even with the high overpotential (at -1.1 eV around 6% current efficiency) and no methanol

formation observed. However, Pd-PANI as a catalyst dramatically increase the production of HCOOH instead of H$_2$(at -1.1 eV around 23% current efficiency). At low external potential (< 0.5 eV) no methanol formation had been observed. However, after -0.5 eV methanol starts forming in reaction mixture. The current efficiency of MeOH formation is maximum (7%) at -0.9 eV. The decrease in genesis of MeOH had been observed at -1.1 eV due to trace amount of CO formation at high external potential[9, 10].

So far to the best of our knowledge no such detailed investigation has been done to understand microscopic mechanism of the formation of HCOOH over MeOH or CO. Understanding of what electronic properties are affecting the selectivity and improving the production of HCOOH may help to design a new catalyst for CO$_2$ conversion. So this work aims to study the role of Pd-PANI in the formation of HCOOH and CH$_3$OH rather than H$_2$ using density functional theory (DFT). First we try to understand the interaction of Pd with PANI then adsorption of CO$_2$ on PANI, Pd and Pd-PANI. Then we study the thermodynamic stability of different possible intermediates. Finally, we propose a probable path for formic acid and MeOH formation.

This thesis is organized as follows: A summary of theory and computational methods is provided in the second chapter. Some practical aspects of density functional theory (DFT) also has been discussed including solvent effect and modeling of the system. The third chapter consists of results and discussions which includes the interaction of Pd and PANI followed by CO$_2$ adsorption on them. Possible mechanistic pathways for formic acid and methanol formation and then the thermodynamic stability of metastable states have been explored. At the end of the chapter, concluding remark, comparison with the experiment and reactive intermediates involved in the reaction. In chapter four we discuss the future directions of the work such as incorporation of zero point energy and entropy correction, effect of external potential, pH and more complex model which will be more realistic with the experiments.

Chapter 2

Theory and Computational methods

F OR the investigations we have used Density Functional Theory (DFT) which has become a prominent tool for electronic structure calculation in today's scenario. It is the method to write the many body Schrödinger equation in such a way so that it reduces the dimensionality of Schrödinger equation from 3N to 3. DFT is presently the most successful and also the most promising approach to compute the electronic structure of matter. DFT predicts a great variety of molecular properties such as: structures, vibrational frequencies, atomization energies, electric and magnetic properties, reaction paths etc. within reasonable accuracy with respect to experimental data and at adequate computational cost[11, 12]. The formulation of DFT would be explained in further section.

2.1 Many body Schrödinger equation

The time independent stationary state Schrödinger equation:

$$H_{tot}\Psi_{tot}(\mathbf{r}, \mathbf{R}) = E_{tot}\Psi_{tot}(\mathbf{r}, \mathbf{R}) \tag{2.1}$$

where H$_{tot}$ is the Hamiltonian and for many body system can be written as:

$$
\begin{aligned}
H_{tot} = \sum_A -\frac{\hbar^2}{2M_A}\nabla^2_{\mathbf{R}_A} + \sum_B -\frac{\hbar^2}{2m_i}\nabla^2_{\mathbf{r}_i} + \frac{1}{4\pi\epsilon_o}\sum_{A>B}\frac{+e^2 Z_A Z_B}{|\mathbf{R}_A - \mathbf{R}_B|} \\
+ \frac{1}{4\pi\epsilon_o}\sum_{i>j}\frac{-e^2}{|\mathbf{r}_i - \mathbf{r}_j|} + \frac{1}{4\pi\epsilon_o}\sum_{i,A}\frac{-e^2 Z_A}{|\mathbf{r}_i - \mathbf{R}_A|},
\end{aligned}
\tag{2.2}
$$

where $\sum_A -\frac{\hbar^2}{2M_A}\nabla^2_{\mathbf{R}_A}$ and $\sum_A -\frac{\hbar^2}{2m_i}\nabla^2_{\mathbf{r}_i}$ are kinetic energies of nuclei and electrons respectively, $\frac{1}{2}\frac{1}{4\pi\epsilon_o}\sum_{A\neq B}\frac{+e^2 Z_A Z_B}{\left|\mathbf{R}_A-\mathbf{R}_B\right|}$ and $\frac{1}{2}\frac{1}{4\pi\epsilon_o}\sum_{i\neq j}\frac{-e^2}{\left|\mathbf{r}_i-\mathbf{r}_j\right|}$ are coulomb interaction between nuclei-nuclei and electron-electron respectively and the last term $\frac{1}{4\pi\epsilon_o}\sum_{i,A}\frac{-e^2 Z_A}{\left|\mathbf{r}_i-\mathbf{R}_A\right|}$ is coulomb interaction between electron and nuclei. In equation 2.1 $\Psi_{tot}(\mathbf{r}, \mathbf{R})$ contains all the information about the system which can be ever known. However it is impossible solve the Schrödinger equation analytically due to electron-electron and electron-nuclei interaction[12, 11]. Many approximation have been made to solve it.

2.2 Born-Oppenheimer approximation

From equation (2.2), H_{tot} can be written as:

$$H_{tot} = T_n + T_e + V_{nn} + V_{ee} + V_{ne}. \tag{2.3}$$

Here T_n is the kinetic energy of nuclei, T_e is the electronic kinetic energy, V_{ne} is the coulombic attraction between nuclei and electron, V_{ee} and V_{nn} is the coulombic repulsion between electrons and nuclei respectively. Now summing up the terms involving electrons, equation (2.3) can be rewritten as

$$H_{tot} = T_n + H_{ele} + V_{nn}, \text{where } H_{ele} = T_e + V_{ne} + V_{ee}. \tag{2.4}$$

Here T_n and V_{nn} are dependent on nuclei positions and H_e, which represents the electronic hamiltonian, has parametrical dependence on nuclei position. As we know that the mass of nuclei is much larger than the mass of electron, we can approximate the motion of nuclei as static compared to the motion of electron. Thus, in equation (2.4) T_n and V_{nn} will be constant for a fixed R, which allows us to solve the electronic part of hamiltonian independently given by

$$H_{ele}\Psi_{ele}(\mathbf{r}; \mathbf{R}) = E_{ele}\Psi_{ele}(\mathbf{r}; \mathbf{R})$$

The eigen value so obtained, E_{ele}, then serves as a potential in the total hamiltonian in (2.6) with the corresponding total wavefunction given by[13],

$$\Psi_{tot}(\mathbf{r}, \mathbf{R}) = \sum_{i=1}^{\infty} \Psi_{ni}(\mathbf{R})\Psi_{ele}(\mathbf{r}; \mathbf{R}) \tag{2.5}$$

$$(T_n + E_j(\mathbf{R}))\Psi_{nj}(\mathbf{R}) = E_{tot}\Psi_{nj}(\mathbf{R}) \tag{2.6}$$

2.3 Density Functional Theory

Even with the static nuclei, the problem of solving the electronic wave function remains unsolvable due to the presence of non-local term like electron-electron repulsive interaction. DFT allow us to reduce the variables of the many-body Schrödinger equation from 3N to 3 according to the Hohenberg-Kohn theorems[12, 14].

2.3.1 Hohenberg and Kohn Theorems

Theorem 1: *For any system of interacting particles in an external potential $V_{ext}(r)$, the density is uniquely determined (in other words, the external potential is a unique functional of the density and vice versa)*[15].

Proof: Let us assume that there were two potentials V_{ext} and V'_{ext} which corresponds to same density $\rho(\mathbf{r})$ for it's ground state we would have two Hamiltonian's H and H' whose ground-state densities were the same although the normalized wave functions Ψ and Ψ' would be different. Taking Ψ' as a trial wave function of Hamiltonian H, E_o and E'_o are the eigenvalues of exact ground state wave functions.

$$E_o < \left\langle \Psi'|H|\Psi' \right\rangle = \left\langle \Psi'|H'|\Psi' \right\rangle + \left\langle \Psi'|H - H'|\Psi' \right\rangle \tag{2.7}$$

$$E_o < E'_o + \left\langle \Psi'|T + V_{ee} + V_{ext} - T - V_{ee} - V'_{ext}|\Psi' \right\rangle \tag{2.8}$$

$$E_o < E'_o + \int \rho(\mathbf{r})\{V_{ext} - V'_{ext}\}d\mathbf{r} \tag{2.9}$$

Similarly,

$$E'_o < E_o - \int \rho(\mathbf{r})\{V_{ext} - V'_{ext}\}d\mathbf{r} \tag{2.10}$$

from equation 2.9 and 2.10 we get

$$E_o + E'_o < E'_o + E_o \Rightarrow 0 < 0 \tag{2.11}$$

This concludes the proof that there cannot be two different external potential that gives rise to the same ground state density is uniquely determined by the external potential[15]. Now,

we can write the total energy in terms of ground state electron density (ρ_o):

$$E_o[\rho_o] = T[\rho_o] + E_{ee}[\rho_o] + E_{ext}[\rho_o], \tag{2.12}$$

where $E_{ext}[\rho_o]$ is comes from external potential $E_{ext}[\rho_o] = \int \rho(\mathbf{r}) V_{ext} d\mathbf{r}$. So now total energy can be written as:

$$E_o[\rho_o] = \left\{ \int \rho(\mathbf{r}) V_{ext}(\mathbf{r}) d\mathbf{r} \right\} + \left\{ T[\rho_o] + E_{ee}[\rho_o] \right\} \tag{2.13}$$

here the first term in the equation 2.13 is system dependent and second one is universally valid (independent of V_{ext}), which is known as *Hohenberg-Kohn functional* $F_{HK}(\rho_o)$, so we can write

$$E_o(\rho_o) = \int \rho(\mathbf{r}) V_{ext}(\mathbf{r}) dr + F_{HK}(\rho_o) \tag{2.14}$$

now if we know the form of F_{HK}, we can solve the Schrödinger equation exactly and the universal function is completely independent of the system taken into account. However, the explicit form of the two terms i.e $T[\rho_o]$ and $E_{ee}[\rho_o]$ is not known. $E_{ee}[\rho]$ can be written as:

$$E_{ee}[\rho] = \frac{1}{2} \int \int \frac{\rho(\mathbf{r_1}) \rho(\mathbf{r_2})}{\mathbf{r}_{12}} d\mathbf{r_1} d\mathbf{r_2} + E_{ncl}[\rho] = J[\rho] + E_{ncl}[\rho] \tag{2.15}$$

where

$$\rho(\mathbf{r}) = \langle \Psi_o | \rho | \Psi_o \rangle = \int \prod_{i=1}^{N} d\mathbf{r}_i |\Psi_o(r_1 r_2 r_3 ... r_N)|^2$$

and

$$N = \int \rho(\mathbf{r}) dr \tag{2.16}$$

$E_{ncl}[\rho]$ represents the *non-classical* contribution of electron-electron interaction which contains all the effects of self-interaction, exchange and coulomb correlation. The explicit form of the expression for this functional is still not known. Only the ground state density contains the information about positions and charges of the nuclei which allows the mapping from density to an external potential[11, 12].

Theorem 2: *A universal functional for the energy $E[\rho(\mathbf{r})]$ can be defined in terms of the density. The exact ground state is the global minimum value of this functional*[15].

Proof: The ground state energy can be obtained variationally: the density that minimizes the total energy is the ground state energy and the corresponding density would be the exact ground state density.

$$E_o \leqslant E[\rho] = T[\rho] + E_{ext}[\rho] + E_{ee}[\rho] \tag{2.17}$$

10

That means for any trial density $\rho(\mathbf{r})$ which satisfies the boundary condition $\rho(\mathbf{r}) \geqslant 0$, $\int \rho(\mathbf{r}) d\mathbf{r} = N$, and associated with external potential V_{ext} the energy obtained will be an upper bound of the true ground state energy E_o. Any trial density $\rho(\mathbf{r})$ defines it's Hamiltonian H and its own wave function Ψ and this wave function now can be taken as a trial wave function for the Hamiltonian generated from true external potential V_{ext}[15].

$$\left\langle \Psi^{'} | H | \Psi^{'} \right\rangle = T[\rho] + V_{ee}[\rho] + \int \rho(\mathbf{r}) V_{ext} d\mathbf{r} = E[\rho] \geqslant E_o[\rho_o] = \left\langle \Psi_o | H | \Psi_o \right\rangle \qquad (2.18)$$

where ρ_o is exact ground state density and Ψ_o is exact ground state wavefunction.

2.3.2 Kohn-Sham ansatz

A year after the ground breaking paper by Hohenberg and Kohn, Kohn and Sham suggested a practical approach to compute the Hohenberg-Kohn functional $F_{HK}[\rho(\mathbf{r})] = T[\rho_o] + E_{ee}[\rho_o]$. They mapped the system of interacting electrons onto a fictitious system of non-interacting ones having the same electron density as that of the interacting system. Earlier the problem was about an exact expression of kinetic energy in the form of density so they proposed to obtain the exact kinetic energy of the non-interacting reference system with the same density as the real and interacting one. Therefore, they write the variational problem for the Hohenberg-Kohn density-functional, introducing a Lagrange multiplier μ to constrain the number of electrons N[16, 11].

$$\delta \left[F[\rho(\mathbf{r})] + \int d\mathbf{r} V_{ext} \rho(\mathbf{r}) - \mu \left(\int d\mathbf{r} \rho(\mathbf{r}) - N \right) \right] \qquad (2.19)$$

Now $F[\rho(\mathbf{r})]$ can be written as :

$$F[\rho(\mathbf{r})] = T_s[\rho(\mathbf{r})] + \frac{1}{2} \int d\mathbf{r} d\mathbf{r}^{'} \frac{\rho(\mathbf{r})\rho(\mathbf{r}^{'})}{\mathbf{r} - \mathbf{r}^{'}} + E_{ext}[\rho(\mathbf{r})] \qquad (2.20)$$

where $T_s[\rho(r)]$ is the kinetic energy of non-interacting gas with the density of $\rho(\mathbf{r})$, the second term is classical Hartree term and the last one is the exchange-correlation term which contains the non-classical electrostatic interaction energy and the difference between kinetic energy of interacting and non-interacting system. The last term is small fraction of total energy so it

can be approximated. Now equation (2.19) can be written as:

$$\frac{\delta T_s[\rho(\mathbf{r})]}{\delta\rho(\mathbf{r})} + V_{KS}(\mathbf{r}) = \mu \tag{2.21}$$

in which $V_{KS}(\mathbf{r})$ can be written as:

$$V_{KS}(\mathbf{r}) = \int \frac{d\mathbf{r}'\rho(\mathbf{r}')}{\mathbf{r} - \mathbf{r}'} + V_{xc}(\mathbf{r}) + V_{ext}(\mathbf{r}) \tag{2.22}$$

and exchange-correlation (V_{xc}) can be given by:

$$V_{xc}(\mathbf{r}) = \frac{\delta E_{xc}[\rho(\mathbf{r})]}{\delta\rho(\mathbf{r})} \tag{2.23}$$

now to find the ground state density $\rho_o(\mathbf{r})$ for non-interacting system, we simply solve the single electronic Hamiltonian.

$$\left[-\frac{1}{2}\nabla^2 + V_{KS}(\mathbf{r})\right]\psi_i(\mathbf{r}) = \epsilon_i\psi_i(\mathbf{r}) \tag{2.24}$$

For N single particle states $\psi_i(\mathbf{r})$ with the energy ϵ_i constructing the density from:

$$\rho(\mathbf{r}) = \sum_{i=1}^{N}|\psi_i(\mathbf{r})|^2 \tag{2.25}$$

and the non-interacting kinetic energy is;

$$T_s[\rho(\mathbf{r})] = \sum_{i=1}^{N}\int d\mathbf{r}\psi_i^*(\mathbf{r})\psi_i(\mathbf{r}) \tag{2.26}$$

V_{KS} Kohn-Sham potential depends on density $\rho(\mathbf{r})$ that means it is necessary to solve these equations self-consistently, which is initiated by choosing an initial density $\rho(\mathbf{r})$ thereby constructing the Schrödinger equation from it, after which solving the latter and calculating the resultant density. Then a new Schrödinger equation is constructed and so on, until the density does not change appreciably any more. The energy of non-interacting system could be written as:

$$\sum_{i=1}^{N}\epsilon_i = T_s[\rho(\mathbf{r})] + \int d\mathbf{r}\rho(\mathbf{r})V_{KS}(\mathbf{r}) \tag{2.27}$$

$$= T_s[\rho(\mathbf{r})] + \int \int \frac{d\mathbf{r}d\mathbf{r}' \rho(\mathbf{r})\rho(\mathbf{r}')}{\mathbf{r} - \mathbf{r}'} + \int d\mathbf{r}\rho(\mathbf{r})V_{xc}(\mathbf{r}) + \int d\mathbf{r}\rho(\mathbf{r})V_{ext}(\mathbf{r}) \quad (2.28)$$

which, compared to the interacting system, double-counts the Hartree energy and over-counts the exchange-correlation energy so that the interacting energy is:

$$E = \sum_{i=1}^{N} \epsilon_i - \int d\mathbf{r}\rho(\mathbf{r})V_{ext}(\mathbf{r}) - \frac{1}{2} \int \int \frac{d\mathbf{r}d\mathbf{r}' \rho(\mathbf{r}')\rho(\mathbf{r})}{|\mathbf{r} - \mathbf{r}'|} + E_{xc}[\rho] \quad (2.29)$$

2.3.3 Exchange -Correlation functional

Now the problem reduces to determine the $E_{xc}[\rho]$ term in the Kohn-Sham density functional expression, and this term is also not known exactly. However it is possible to make simple approximations for the exchange-correlation energy which works fairly well and the simplest of these is the *local density approximation*(LDA). The LDA approximates the XC functional at any position r. as the XC energy per electron in a uniform homogeneous electron gas of density $\rho(\mathbf{r})$[13, 11]. The LDA expression for E_{xc} is:

$$E_{xc} = \int d\mathbf{r}\epsilon_{xc}[\rho(\mathbf{r})]\rho(\mathbf{r}) \quad (2.30)$$

where $\epsilon_{xc}[\rho(\mathbf{r})]$ is the exchange correlation energy of homogeneous electron gas of density $\rho(\mathbf{r})$. Then exchange correlation potential $V_{xc}(\mathbf{r})$ takes the form of:

$$V_{xc}(\mathbf{r}) = \frac{\delta E_{xc}[\rho(\mathbf{r})]}{\delta \rho(\mathbf{r})} = \epsilon_{xc}[\rho(\mathbf{r})] + \rho(\mathbf{r})\frac{d\epsilon_{xc}(\rho)}{d\rho}\bigg|_{\rho=\rho(\mathbf{r})} \quad (2.31)$$

LDA is remarkably accurate but often fails when the electrons are strongly correlated, as in systems containing d and f orbital electrons.

GGA approximation not only use the information about the density $\rho(\mathbf{r})$ at a particular point r but also supplement the density with the information about the gradient of charge density, $\nabla\rho(\mathbf{r})$ in order to take into the account for non-homogeneity of the true electron density, so we can write the exchange correlation energy in the following form:

$$E_{xc}^{GGA}[\rho_\alpha, \rho_\beta] = \int f\left(\rho_\alpha, \rho_\beta, \nabla\rho_\alpha, \nabla\rho_\beta\right)d\mathbf{r} \quad (2.32)$$

Becke introduced a successful hybrid-functional :

$$E_{xc}^{hyb} = \alpha E_{xc}^{KS} + (1 - \alpha) E_{xc}^{GGA} \tag{2.33}$$

where E_{xc}^{KS} is the exchange correlation calculated with the exact KS wave-function. E_{xc}^{GGA} is an appropriate GGA and α is a fitting parameter. GGA and hybrid approximations has minimize the errors of LDA approximation and the energies of standard set of small molecules by a factor 3-5[13, 17].
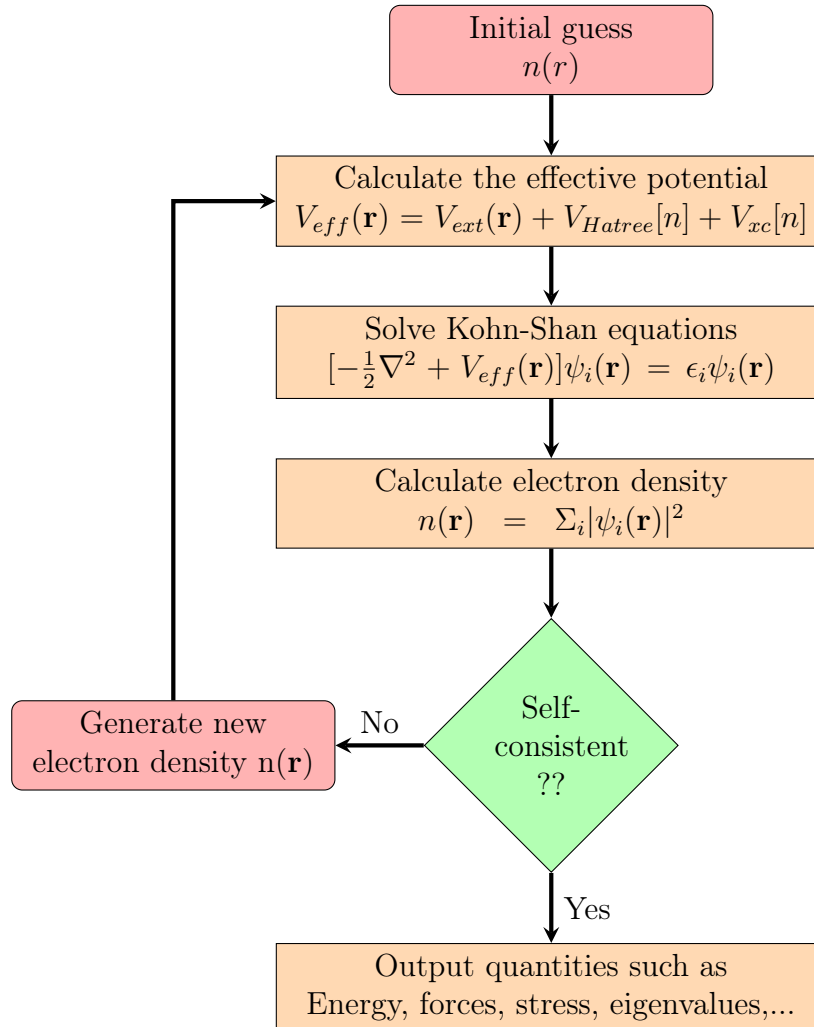
Figure 2.1: This flow chart shows self-consistency cycle for the solution of Kohn-Sham equations.

2.3.4 Self-consistency cycle

Now to get the eigenfunction of KS equations we need to solve the KS equations self-consistently. The self-consistency cycle has been given in figure:2.1. First step is to choose the basis set and initial guess for density $n(r)$ then construct V_{eff}, $V_{eff} = V_{ext} + V_H + V_{xc}$ with the V_{eff} solve the KS equations, calculate new electron density. If convergence criteria is met, one proceeds to calculate total energies , force etc. If convergence is not achieved, the new density is used as the new guess and the procedure is repeated.[17].

2.3.5 Plane-wave basis set

Kohn-Sham orbitals can be expanded in terms of plane waves basis set. For periodic system use of plane wave basis set is useful. The solution of Schrödinger equation for periodic system will satisfy the Bloch's theorem. The electronic wave-function within the constrain of perfectly periodic potential can be written as:

$$\Psi_k(\mathbf{r}) = e^{ik\bullet\mathbf{r}}u_k(\mathbf{r}) \tag{2.34}$$

where $u_k(\mathbf{r})$ possesses the same periodicity as the unitcell and can be expanded as:

$$u_k(\mathbf{r}) = \frac{1}{\Omega} \sum_{\mathbf{G}} C_{\mathbf{k},\mathbf{G}} e^{i\mathbf{G}\bullet\mathbf{r}} \tag{2.35}$$

where G is the vector in reciprocal space and is defined by $\mathbf{G} \cdot \mathbf{R} = 2\pi m$, $\mathbf{R}$ is the lattice vector in real space and Ω is the unitcell volume. From equation (2.34) and (2.35) we can write Ψ_k as:

$$\Psi_{\mathbf{k}}(\mathbf{r}) = \frac{1}{\Omega} \sum_{\mathbf{G}} C_{\mathbf{k},\mathbf{G}} e^{i(\mathbf{G}+\mathbf{k})\bullet\mathbf{r}} \tag{2.36}$$

The plane waves that appear in the above expansion can be represented as a grid in k-space. Each electron occupies a state of definite $\mathbf{k}$, the infinite number of electrons within the solid gives rise to an infinite number of k-points. So in principle we need an infinite number of plane waves. However in practice higher order terms of Fourier component have negligible contribution[18]. So we can truncate the expansion at some value of $|\mathbf{k} + \mathbf{G}|$ and the way is:

$$E_{cut} = \frac{\hbar^2|\mathbf{k} + \mathbf{G}|^2}{2m} = \frac{\hbar^2}{2m}\mathbf{G_{cut}}^2 \tag{2.37}$$
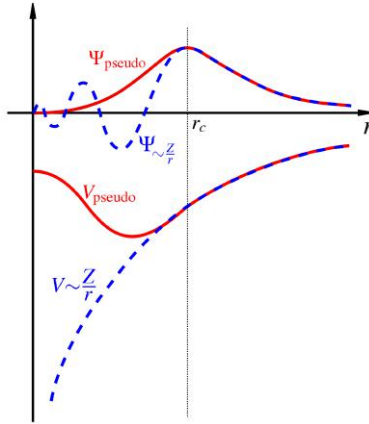
Figure 2.2: Pseudopotential sketch

After this truncation the infinite sum of plane waves reduces to

$$\Psi_{\mathbf{k}}(\mathbf{r}) = \frac{1}{\Omega} \sum_{|\mathbf{G}+\mathbf{k}|<\mathbf{G_{cut}}} C_{\mathbf{k},\mathbf{G}} e^{i(\mathbf{G}+\mathbf{k})\bullet\mathbf{r}} \tag{2.38}$$

2.3.6 Pseudopotential

From the perspective of chemical interaction core electrons (very tightly binded to the valence) do not involve in the bonding and other physical properties which define the system. Those are mostly influenced by relatively loosely bounded valence electrons, So we can ignore the core region. Further due to constrain of Pauli exclusion principle (orthogonality condition) the outer shell valence orbitals are oscillating near the core region. To represent such an highly oscillating function one need a large number of plane waves making it computationally expensive. To smoothen the orbitals at core we replace the all-electron wavefunction with a pseudo wavefunction. Further the core electrons are removed and the nucleus is replaced by an effective nucleus whose charge is screened by the core electrons. Core region of the wavefunction will be defined till r_c, thereafter valence states should be identical to all electron wave-function or potential (figure:2.2). r_c will be defined in such a way so that it can mimic the physical properties of the system significantly accurate with the least computational cost[13, 14].

2.4 SCCS model

To get the actual insight about the minimum energy paths, solvent effect should not be neglected because the experiment has been performed in aqueous condition and solvent can change things significantly. To include solvent, we have used Quantum-Environ with self-consistent continuum solvation (SCCS) model[19]. Here dielectric medium modeled self consistently on the electronic density of solute by

$$\epsilon(\mathbf{r}) = \epsilon(\rho^{ele}(r))$$

It is defined in such a way that dielectric effect should not be present at the inner part of solute where electron density is very high and smoothly goes to bulk dielectric constant as electron density (of solute) goes to zero, represented as (schematic shown in figure:2.3):

$$\epsilon_{\epsilon_0, \rho_{min}, \rho_{max}}(\rho^{ele}) = \begin{cases} 1 & \rho^{ele} > \rho_{max} \\ s(\rho^{ele}) & \rho_{min} < \rho^{ele} < \rho_{max} \\ \epsilon_0 & \rho^{ele} < \rho_{min} \end{cases} \tag{2.39}$$

where ρ^{ele} is the electron-density of solute and ϵ_0 is bulk dielectric constant.
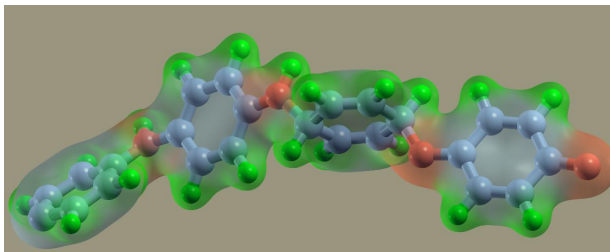
Figure 2.3: Polyaniline with SCCS model, surface is showing the region where dielectric function varies smoothly and it will be decided by ρ_{max} and ρ_{min}, gray color represent $\epsilon(\rho^{ele}) = \epsilon_0$

2.5 Computational hydrogen electrode

Nørskov and his co-workers have observed the thermodynamics of cathode reaction where reduction of CO_2 occurs as a function of external potential. They have shown that the reaction over-potential is directly correlated with the electron-proton transfer at the cathode

site where adsorbate is strongly binded with surface. Since it i not possible to calculate the free energy of an electron and proton, they have setup the standard hydrogen electrode potential as reference. $2(H^+ + e^-) \rightarrow H_2$ as zero electrode potential, which means the energy of $(H^+ + e^-)$ is equal to $\frac{1}{2}H_2$.

2.6 Computational details

To find the ground state (minimum energy structure) of the species an ab initio quantum calculation was run for the intermediates, reactants and products. Spin polarized calculations have been performed using the open source Quantum ESPRESSO software[20]. Perdew Burke Ernzerhof (PBE)[21] exchange-correlation functional has been used within the generalized-gradient approximation (GGA) to describe the electron-electron correlation. We have used ultrasoft pseudopotential to take electron-ion interaction into consideration. Convergence of total energy has been achieved with a $5 \times 1 \times 1$ k-mesh[22] grid, wave-function cutoff of 35 Ry and charge density cutoff of 320 Ry. Long range non-local correlation interaction (vdW) has been included via Grimme's dispersion correction (DFT-D)[23, 24]. To accelerate the calculation Marzari-Vanderbilt (MV)[25] smearing has been used with a smearing width of 0.003 Ry. We have performed charge transfer analysis using density derived electrostatic and chemical (DDEC) net atomic charges which has been implemented in chargemol[26, 27].

Polyaniline (PANI) is a 1-d polymer made of aniline $(C_6H_5NH_2)$. The configuration of PANI changes if pH of the medium changes. Its ability to promote electron-proton transfer made this polymer very valuable. Conductivity of PANI also changes from conducting to semi-conducting depending on its form. PANI exists in three different forms namely perni-graniline (PB), emeraldine base (EB) and leucoemeraldine (LEB). Out of these, LEB is fully reduced, i.e. all the nitrogens are sp^3 hybridized (figure:2.4(A)), EB is partially reduced, i.e. in a monomeric unit half of the nitrogens are sp^2 hybridized and the rest are sp^3 hybridized (figure:2.4(B)) and PB is fully oxidized, i.e. all the nitrogens are sp^2 hybridized (figure:2.4(C)). These configurations are pH dependent[28]. At pH values around 5 to 8, PANI exists primarily as EB. For $pH > 8$ (alkaline medium) it starts converting into PB, while $pH < 5$ (acidic medium) it starts converting into LEB. In our calculations we have taken EB form (figure:2.4) as a monomer unit of the polymeric chain because experiments show that electroreduction happens in slightly acidic medium. So in that atmosphere PANI would exist primarily in EB form.

PANI is modeled by putting an EB monomer in an orthorhoumbic box that is periodically
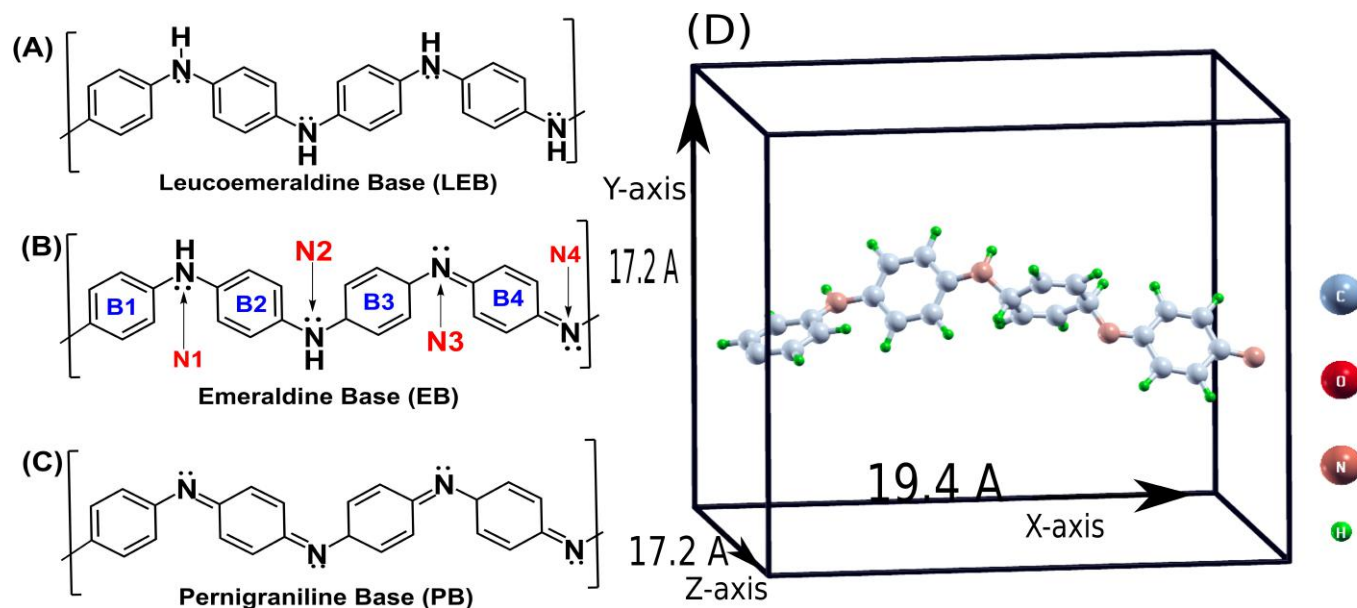
Figure 2.4: Different forms of PANI has been shown in figure. At very high pH it exist as LEB(A) form around neutral pH PANI exist as EB(B) and very high pH it exist as PB(C). (D) represent the monomer model of polymeric chain of PANI.

repeated in space. The chain of the polymer is aligned along the x-axis. Along the direction perpendicular to the chain we have used vacuum of about 12.9 Å along y-axis and 14.0 Å along z-axis to minimize the spurious interaction with its periodic image. Then we performed a relaxation where the unit cell along the polymeric chain is optimized to obtain the polymeric unit-cell length. We find an optimized lattice parameter of 19.4 Å. To check the formic acid and methanol formation possible site for intermediates adsorption on PANI were explored. Further, interaction of Pd adatom on PANI has been checked with the possible adsorption sites. To include the effect of solvent on the reaction energetics self-consistent continuum solvation (SCCS) model has been used as implemented in Quantum Environ[19]. SCCS model has been described in section 2.4.

2.7   Adsorption and relative energy calculation

Adsorption energies has been calculated by equation given below:

$$E_{adsorption} = E_{adsorbent+adsorbate} - E_{adsorbate} - E_{adsorbent}$$

where $E_{adsorbent} = E_{PANI/Pd-PANI}$ and $E_{adsorbate} = E_{CO_2/intermediates}$ To calculate the relative stability of the intermediates we rescaled the total energies by a common reference because the number of atoms are not same while moving from one intermediate to the next.

Chapter 3

Results and Discussions

I NITIALLY all the reaction energies of PANI, Pd-PANI and intermediates were calculated in vacuum. The energies for Pd-PANI and intermediates were obtained by taking the structures of different Pd-PANI, intermediates and performing a structural relaxation in order to find their ground state structure and total energy. In most of the cases, reaction-site has been observed on Pd of Pd-PANI and N of PANI. First we have shown the interaction of Pd with PANI then the reduction of CO_2 to formic acid on PANI and Pd-PANI and finally the conversion of CO_2 to MeOH on Pd-PANI. For all cases the solvent effect and comparison with gas-phase also has been shown.

3.1 Interaction of Pd and PANI

The Pd-PANI interface has been modeled using PANI and a Pd adatom on top of it. We have considered all the possible conformers (feasible adsorption sites) for binding of Pd on PANI. In its most stable configuration Pd simultaneously binds with one of the sp^2 hybridized nitrogen (N_3) and the C-C double bond of the quinoid moiety adjacent to it with a binding energy of -2.15 eV (figure:3.1A). The other possible structures have been given in the appendix (table:A.6)

When Pd interacts with PANI some conformational changes occurs on PANI. The C=C of quinoid moiety to which Pd binds is stretched by about 0.06 Å, which shows that the double bond character of C=C is changing to partial-double bond. So we expect that the charge density should deplete from this bond because π-bond is more electron rich than σ-bond. To check this we have plotted the charge density difference before and after interaction between Pd and PANI. From the charge transfer plot (figure:3.1(B)) we find depletion of charge density
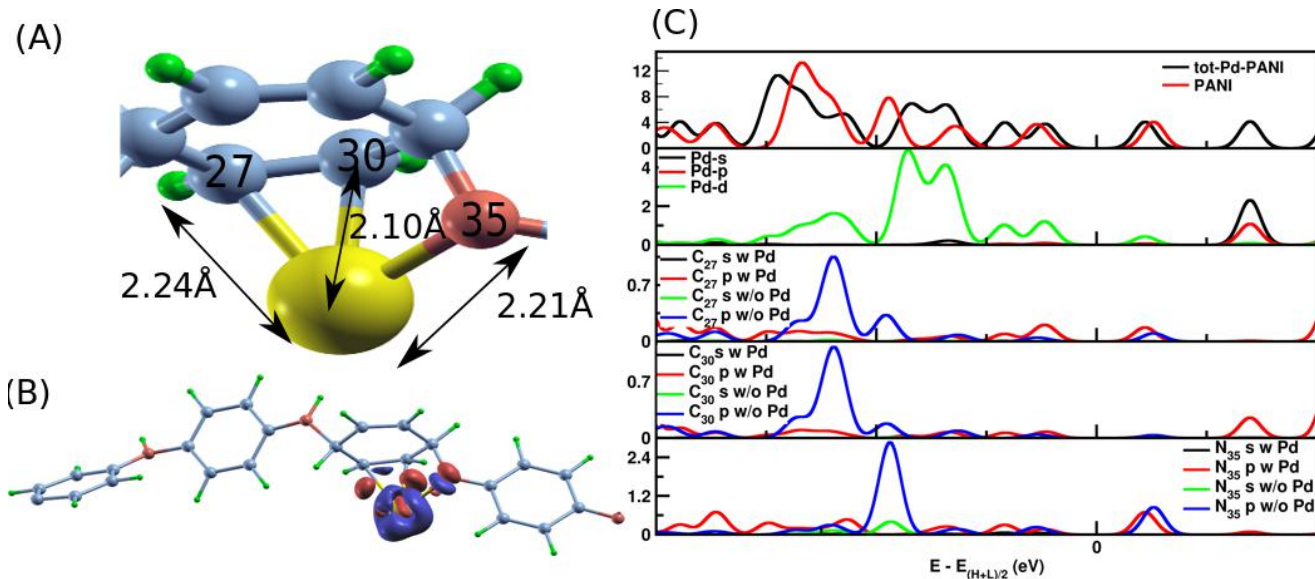
Figure 3.1: (A) Thermodynamically most stable Pd-PANI structure and the corresponding bond lengths has been shown. (B) Plot of charge density difference isosurface $\Delta\rho_{Pd-PANI} = \rho_{Pd-PANI} - \rho_{Pd} - \rho_{PANI}$. Blue color shows charge depletion and red shows charge accumulation. (C) Total Density of states (DOS) and projected ODS of Pd-PANI. First panel shows the total DOS of PANI (red) and Pd-PANI (black). Second panel shows the DOS projected on the s,p,d states of interacting Pd. Third, fourth and fifth panels show the DOS projected on s,p states of C and N atom of PANI that are interacting with Pd, both in presence and absence of Pd.

from the C=C double bond which supports the character of partial double bond. We find that there is some charge depletion (about 0.12e^-) from Pd atom and accumulation on both the C-Pd bond and slightly on the nitrogen. Figure:3.1(C) shows the total DOS of Pd-PANI and PANI and those of interacting atoms projected on their atomic orbitals (AOs). In the first panel of atom projected DOS we find there are occupied new states at around -0.8 eV which are coming from Pd's d orbitals that at 1.5 eV is arising due to Pd's s and p states (figure:3.1(C)). In the third panel of atom projected DOS new states emerges at -0.5 eV and -0.8 eV due to hybridization between Pd and C's of PANI. C_{30} have some new states at 1.5 eV which mainly comes from the interaction of Pd's s and p states with C. In atom projected DOS we have not observed much change in s states to C and N which indicates interaction occurs primarily through p states of C, N and d, s of Pd. After adsorption of Pd on PANI bandgap increases slightly.
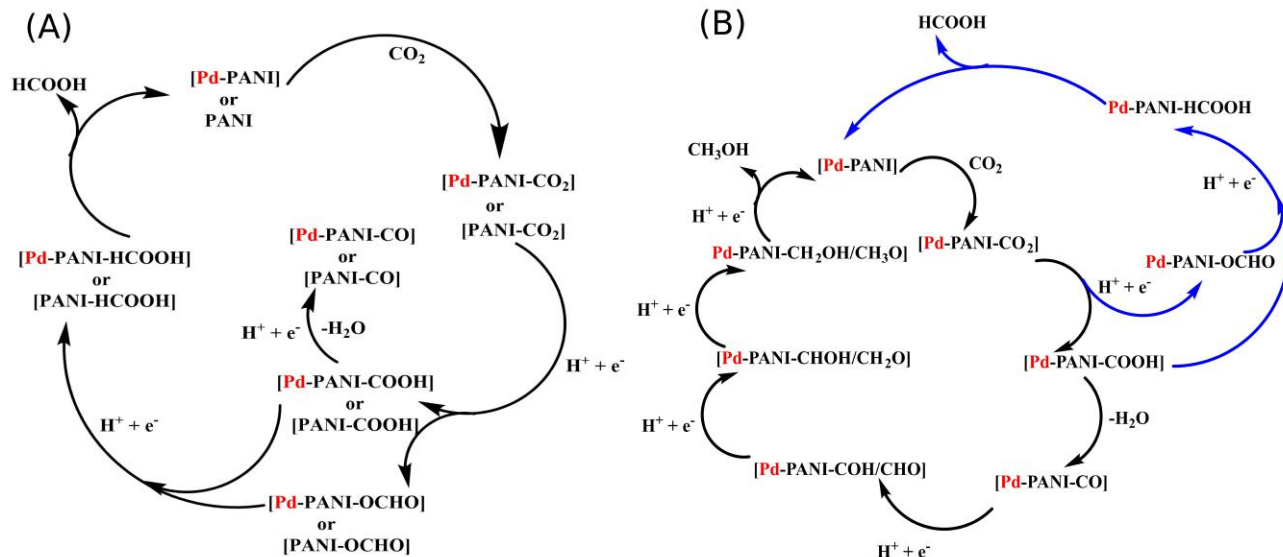
Figure 3.2: Catalytic cycle of CO$_2$ conversion on PANI(A) and Pd-PANI(B) has been shown. Blue arrows shows the formic acid formation on Pd-PANI and black shows the MeOH formation.

3.2 Catalytic cycle for CO$_2$ conversion

Norskov *et al.* have shown the HCOOH formation pathways[29]. Schematic of the mechanism has been shown in figure:3.2(A). The first step in electroreduction of CO$_2$ is the adsorption of CO$_2$ on adsorbent, that in our case is PANI or Pd-PANI. In the next step, another electron-proton transfer takes place and forms either *COOH or *OCHO. Another electron-proton transfer to these adsorbed species leads to the formation of HCOOH[30]. Schematics of the reduction reaction on Pd-PANI has been shown in figure:3.2(B).

For CH$_3$OH formation, the first three steps are same as in the formation of HCOOH (till *CO intermediate via *COOH)[31]. Methanol can be formed either reducing *CO or *HCOOH. *HCOOH can accept an electron-proton and lead to the formation of *CHO + H$_2$O. However, *CO accepting an electron-proton could end-up forming either *CHO or *COH. Then three consecutive electron-proton transfer takes place and CH$_3$OH is formed via the following intermediates *CHOH or *CH$_2$O to *CH$_2$OH or *CH$_3$O. Schematic of the mechanism has been shown in figure:3.2(B).

3.3 Reduction of CO$_2$ to Formic acid

In this section we describe the energetics of formation of formic acid on PANI and Pd-PANI. For each of the reaction steps we have considered several possible configurations. Here we present only the most stable ones. Others are reported in appendix (table:A.5).

3.3.1 Formic acid formation on PANI

The first step towards CO$_2$ reduction is adsorption of CO$_2$ on PANI. We have chosen nitrogen sites for the adsorption of CO$_2$ on PANI because nitrogen atoms are well known for trapping gaseous CO$_2$. The possible interaction between CO$_2$ and nitrogen could be n→π*. Our calculations show that in the most stable configuration CO$_2$ adsorbs on PANI through the N$_3$ nitrogen as shown in figure:2.4(B) with a binding energy of -0.26 eV and C−N distance of 3.04 Å. Adsorption of CO$_2$ to PANI through the other N's are about 0.04 eV weaker in energy compared to that of N$_3$. The interaction of CO$_2$ is slightly more with sp^2 hybridized nitrogen due to the ability of the lone pair on N$_3$ to attract the slightly positive charged C-atom of CO$_2$ more efficiently. Adsorption strength of CO$_2$ at the top of benzene and cyclohexadiene rings are negligible (hollow sites). After adsorption of CO$_2$ on PANI the C=O bond length remains almost similar to that in the gas phase (change in bond length around 0.002 Å). CO$_2$ goes to slightly bent state from the linear one and the bond angle changes to 176.6° from 180°.
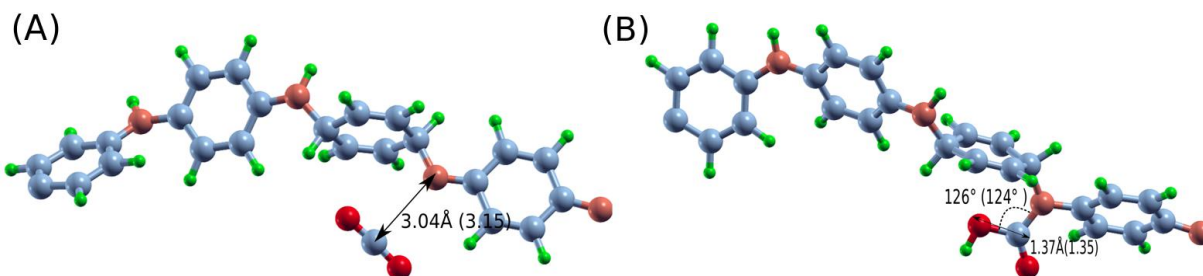
Figure 3.3: (A) Most stable conformation of CO$_2$ adsorption on PANI (B) Most stable configuration of COOH on PANI. The bond lengths and bond angles shown in parenthesis are in presence of solvent.

After including the implicit solvent model interaction becomes slightly because distance between C and N increases from 3.04 Å to 3.15 Å (see figure:3.3) and O-C-O angle also changes from 176.6° to 178°.
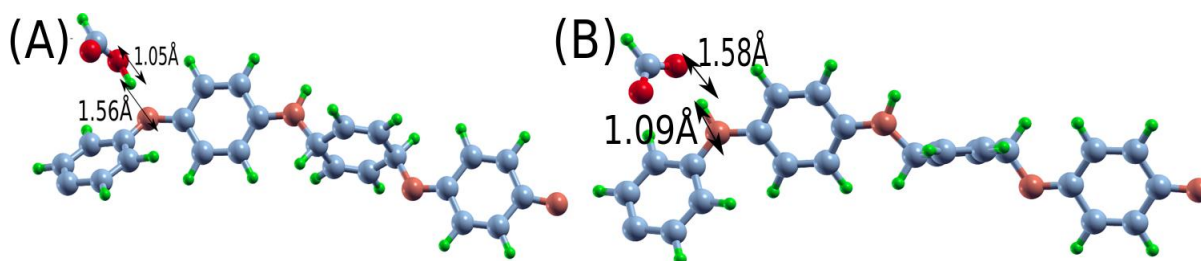
Figure 3.4: (A) OCHO on PANI in gas phase, OH bond length 1.05 Å and N-H bond length 1.56 Å (B) OCHO on PANI in solvent, OH bond length 1.58 Å and N-H bond length 1.09 Å

According to the possible mechanism the next step is electron-proton transfer to PANI-CO₂ and formation of either *COOH or *OCHO takes place. Here the assumption we have made is that electro-proton transfer happens simultaneously. *COOH binds to PANI through the sp² hybridized N_3 atom. The available lone-pair on the nitrogen forms strong sigma bond with that of the C atom of COOH (see figure:3.3(B)). When we include the effect of solvent it further stabilizes the intermediate, C-O bond length slightly decreases by about 0.02 Å and O-C-N bond angle also reduces by about 2°. In case of OCHO, O has an unpaired electron that is resonating on both the oxygen atoms. The lone pair-lone pair (lp-lp) repulsion prevent a strong interaction between OCHO and PANI. In most of OCHO cases two things are happening, OCHO is taking the proton from nitrogen (from N_1 and N_2 figure:2.4(B)) if it has one and forms HCOOH (figure:3.4) or it gives a proton to the nitrogen (N_3 and N_4 figure:2.4(B)) and forms CO₂ (see appendix table:A.2). If it is not possible to donate or accept the proton, it remains as OCHO with almost negligible interaction with PANI (see appendix table:A.2). After including the effect of solvent *OCHO is stabilized through hydrogen bonding between H of N and O of OCHO(figure:3.4(B)).

Now, once *COOH or *OCHO has formed, a proton-electron transfer will take place to form subsequent reaction intermediate. *COOH can accept a proton in two different ways either through carbon or oxygen (which is having hydrogen on it). If *COOH takes a proton at oxygen, it will release H₂O and forms *CO (*COOH + H⁺ + e⁻ → *CO + H₂O). If C atom takes the proton it forms formic acid (*COOH + H⁺ + e⁻ → *HCOOH). However, in *OCHO case there is only one possibility from where it can accept a proton, which is at the oxygen site. So it will lead to the formation of HCOOH.

Possible genesis sites for carbon-monoxide and formic acid have been explored (see the appendix table:A.4). The interaction of CO with PANI is negligible. That means if *COOH forms H₂O and *CO, CO will desorbed. Although the interaction between CO and PANI is very minimal, still N_3 site remain as the most-interacting one. Furthermore, HCOOH
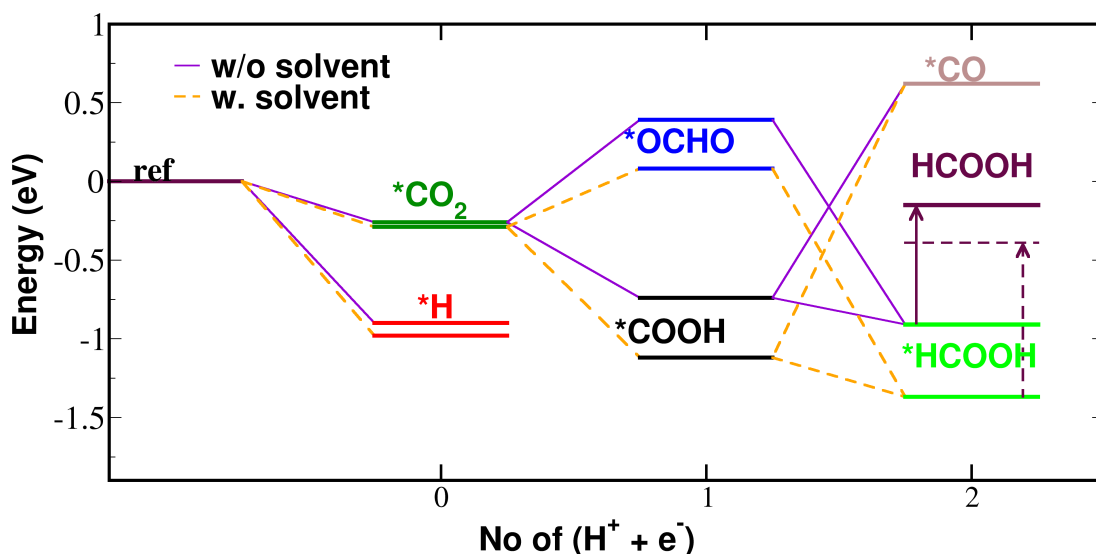
Figure 3.5: Energetics for reduction of CO2 on PANI with solvent and gas phase. The energies are rescaled with respect to that of Pd-PANI+CO_2+H_2

formation also takes place at N_3 site due to the most substantial interaction of HCOOH with PANI was observed at N_3 site.

We have plotted the relative energy diagram for all the intermediates in gas phase on PANI (and in solvent also) for the formic acid formation (figure:3.5). All the energies are rescaled by total energy of PANI + CO_2 + H_2 (PANI(env)+CO_2 + H_2 for solvent) in the gas phase. After adsorption of CO_2 an electron-proton transfer leads to the formation of *COOH, which results in the stabilization of the complex by about -0.48 eV compared to that of *CO_2 (downhill path). In contrast adsorption of *OCHO is endothermic, and the complex is about 0.65 eV higher than *CO_2. Hence, we envisage that formation of formic acid will proceed through the *COOH intermediate. With an electron-proton transfer *COOH either could end-up forming *CO or lead to the creation of *HCOOH. However, the formation of *CO is thermodynamically unfavorable due to the high energy cost of 1.3 eV with respect to *COOH. Hence, it leads to the creation of *HCOOH.

On inclusion of solvent effects we find that the overall reaction pathway remains same. The solvent stabilizes the intermediates and the amount of stabilization depend on the nature of the solute. Change in relative energy as reaction proceeds are shown in the figure:3.5. For PANI−CO_2 case there is no significant change in the structure. However, wherever the interaction is strong the consequence of environment is substantial as in case of *COOH, *OCHO, and HCOOH. *COOH and *HCOOH are stabilized further by -0.38 eV and -0.46 eV respectively when the solvent effects are taken into consideration in our calculation. In

(a) CO_2 on PANI (b) Pd-CO_2 η^1-C mode (c) CO_2 on Pd$-$PANI(η^2-CO mode)
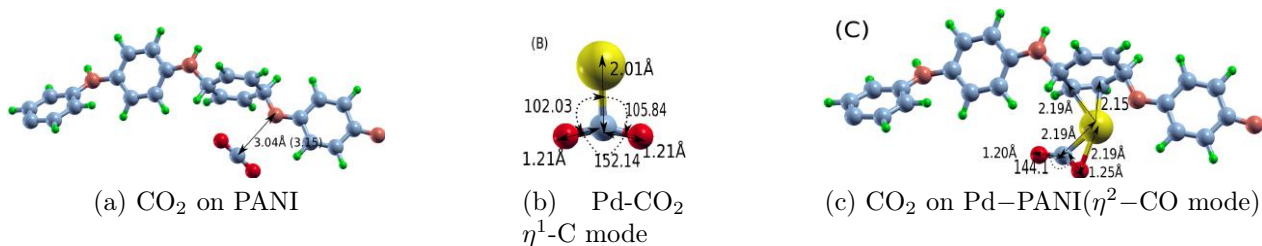
Figure 3.6: Interaction of CO_2 with PANI (a), Pd (B) and Pd-PANI (c). Corresponding bond lengths and bond angles have been shown in the figure.

experiments Weiran Zheng *et. al.* have not observed the formation of *CO on PANI and that can be explained by figure:3.5. This is probably due to the fact that the formation of *CO is thermodynamically unfavorable (uphill path)[10].

3.3.2 Formic acid formation on Pd-PANI

Till now we have discussed about CO_2 conversion on PANI. Here CO_2 reduction on Pd-PANI has been discussed. Similar to PANI first CO_2 will interact with Pd-PANI. It has been observed that CO_2 interacts primarily through Pd of Pd-PANI. The feasible interaction between Pd (of Pd-PANI) and CO_2 can be n$\to \sigma^*$ because CO_2 has an anti-bonding orbital as σ^* and Pd (of Pd-PANI) has its d-orbitals as non-bonding ones. CO_2 interacts with Pd of Pd-PANI through either η^1-C mode or η^2-CO mode[32] (see figure:3.6). Through η^2-CO mode interaction is stronger than η^1-C mode. To know how Pd-PANI is affecting the interaction of CO_2 with adsorbent, a comparison of CO_2 adsorption on PANI, Pd-atom and Pd-PANI has been shown in figure:3.6 and corresponding change in bond lengths and bond angle have been shown in the table:3.1. Interaction with PANI already has been described earlier. While interacting with Pd-atom, C=O bond length changes from 1.17 Å to 1.21 Å and bond angle changes from 180° to 152.14° that means CO_2 gets activated. However, interacting with Pd-PANI CO_2 interacts asymmetrically through C=O. So change in bond length of C=O (directly attached to Pd) is about 0.08 Å and other C=O bond changes around 0.03 Å. Bond angle also changes quite significantly by about 36° for Pd-PANI case. The adsorption energy of CO_2 on Pd-PANI is almost twice (-1.31 eV) to that of Pd-atom (0.65 eV). The reason behind this strong bonding of CO_2 with Pd-PANI compared to Pd-atom is the following. PANI supported Pd can give more electrons (about -0.35 e^-) to the adsorbed CO_2 than Pd-atom (-0.25 e^-). However, Pd-atom is not able to donate the same amount of charge as Pd-PANI to CO_2. So that is why Pd-PANI have stronger binding than Pd-atom with CO_2.

Bond / Angle	CO$_2$	PANI	Pd	Pd−PANI
C=O Å	1.17	1.17	1.21	1.25 (Pd), 1.20
$\angle COC$	180°	176°	152°	144°
B.E (eV)	−	-0.26	-0.65	-1.31

Table 3.1: CO$_2$'s bond-length, bond-angle and interaction energies after interacting with PANI, Pd and Pd-PANI.
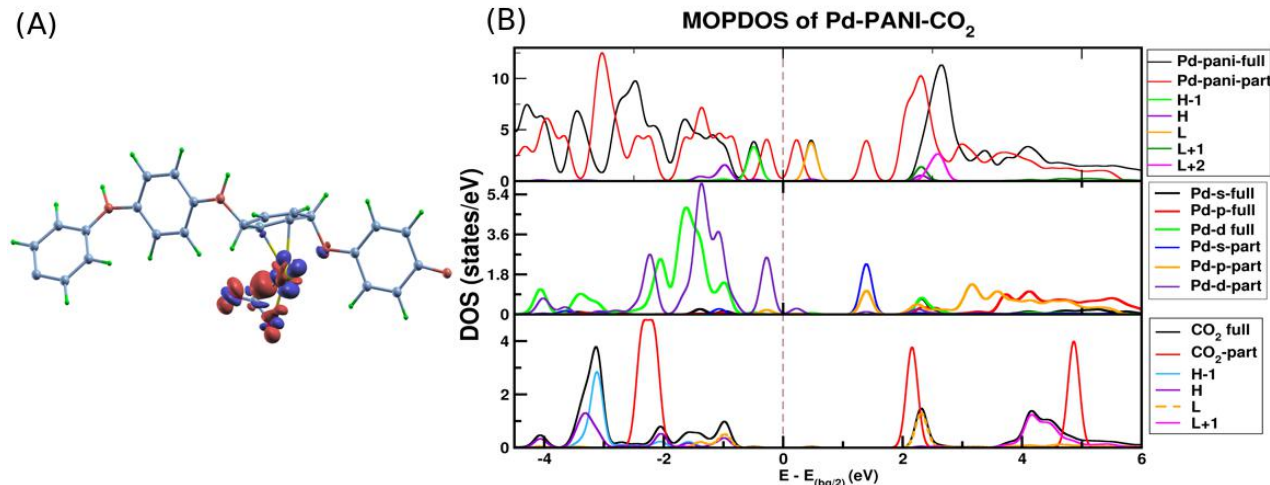
Figure 3.7: (A)Plot of charge density difference isosurface $\rho(r) = \rho_{Pd-PANI-CO_2} - \rho_{Pd-PANI} - \rho CO_2$. Blue color shows charge depletion and red shows charge accumulation. (B) Top panel shows the total DOS of Pd-PANI-CO$_2$ (black curve) and DOS of Pd-PANI (red curve) in the interacting geometry. H, H-1 represents homo, homo-1, and L, L+1 represents lumo, lumo+1. Middle panel shows the DOS projected on Pd d, s, p states. "Full" denotes Pd-PANI-CO$_2$ and "part" shows Pd-PANI or CO$_2$. The bottom panel shows the DOS of Pd-PANI-CO$_2$ projected on the molecular orbitals of CO$_2$.

To understand the interaction of Pd-PANI with CO$_2$, we need to understand what type of orbitals are involved in the bonding and whether there is a charge transfer or not. To understand that we have plotted charge-density difference, the dos projected on molecular-orbitals (mopdos) and atomic charges also have been calculated (figure:3.7). Charge density difference plot shows redistribution of charge density takes place, and there is some charge accumulation on CO$_2$ and charge depletion on Pd-atom and nitrogen of PANI. CT shows that Pd loses 0.11e$^-$ charge and carbon, oxygen (which is connected to Pd) gain 0.19e$^-$ and 0.12e$^-$ charge respectively. The other oxygen also accumulate slight charge 0.05e$^-$. Pd gives it's non-bonded electrons to σ^* orbital of the CO$_2$. This can be confirmed by molecular orbitals projected DOS (figure:3.7(B)). From molecular orbitals projected DOS CO$_2$'s homo is shifted towards lower energy with respect to gas phase CO$_2$ orbitals. Lumo is also occupied
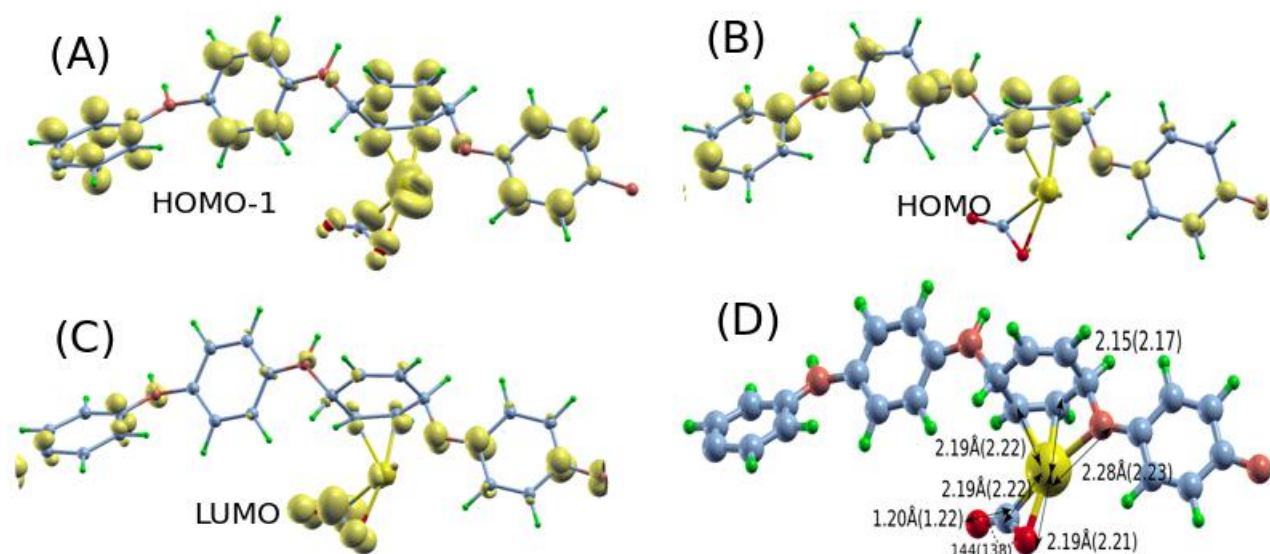
Figure 3.8: Isosurfaces of the ILDOS from -1.3 eV to -0.75 eV (A), from -0.75 eV to -0.22 eV (B), and from 0.17 eV to 0.73 eV (C) of Pd-PANI-CO$_2$ (in first panel of the figure:3.7(B)). These ILDOS are in gas phase. (D) Most stable conformer of Pd-PANI-CO$_2$. Values in the parenthesis are those in presence of solvent.

after the interaction which shows the charge transfer because gas phase CO$_2$'s lumo has now becomes the homo of interacting phase CO$_2$. It is a clear signature of non-bonding orbital to σ^* anti-bonding orbital charge transfer. New states appears at -1 eV in CO$_2$ shows the interaction of CO$_2$ with Pd-d orbitals. To understand what states are involved in Pd-PANI-CO$_2$'s homo and lumo we also have plotted integral local density of states (ILDOS) in the energy window of homo-lumo regime (figure:3.8). We observed here homo of Pd-PANI-CO$_2$ consist of mixture of PANI, Pd and CO$_2$ states (figure:3.8(B)) However, lumo of Pd-PANI-CO$_2$ involves mixture of CO$_2$, Pd and PANI states (figure:3.8(C)). Moreover, proton can also interacts with C=N of PANI (N$_3$ and N$_4$). After including solvent effect adsorption energy of CO$_2$ increases which means interaction getting stronger in solvent. Conformational changes in Pd-PANI-CO$_2$ in solvent medium has been shown in figure:3.8(D). All the bond lengths and bond angles are slightly perturbed. Pd-N bond length is decreased by about 0.05 Å and the O-C-O bond angle is shortened by about 6°. Other bonds are also stretched by about 0.02-0.03 Å.

So now CO$_2$ is in an activated form and adsorbed on Pd-PANI. Next step is an electron-proton transfer which will lead to formation of either *OCHO or *COOH. We explored all possible reactive sites for different configuration on Pd-PANI (see the appendix table:A.2). For Pd-PANI, reaction site has been observed on Pd atom for all the intermediates (without solvent).
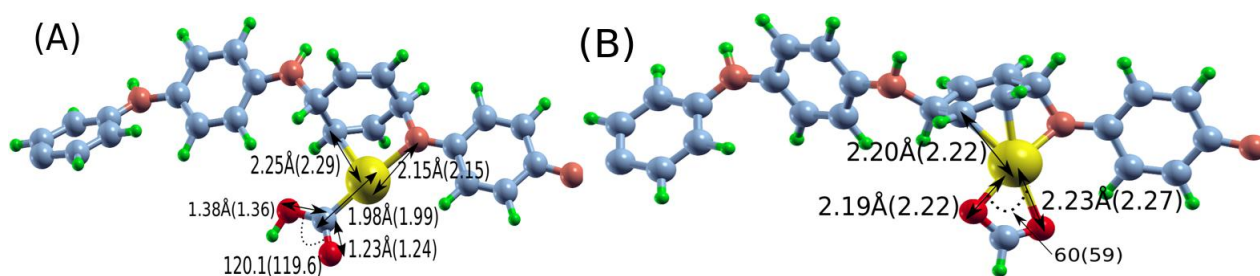
Figure 3.9: Conformational changes in Pd-PANI-COOH and Pd-PANI-OCHO after including solvent (w.r.t gas phase). Values shown in the parenthesis shows the bond length and bond angle in presence of solvent.
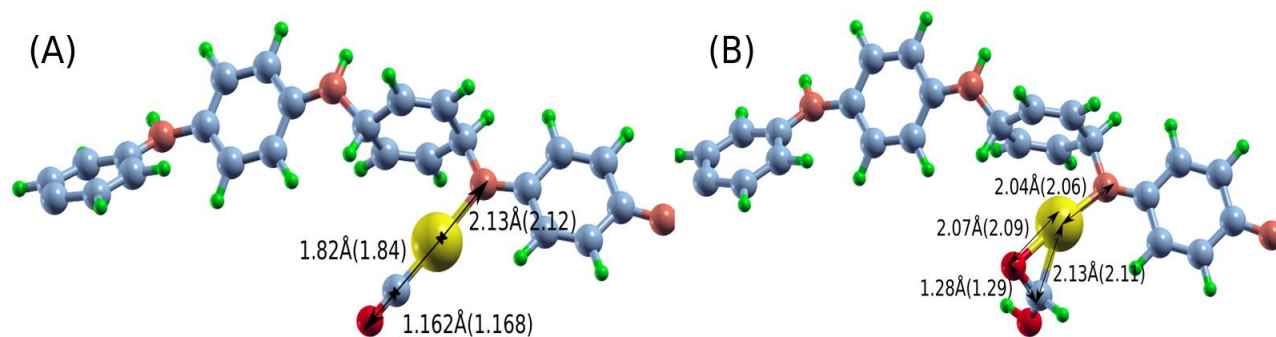
Figure 3.10: Conformational changes in Pd-PANI-CO and Pd-PANI-HCOOH after including solvent (w.r.t gas phase). Values shown in the brackets shows the bond length or bond angle in presence of solvent.

When we include the effect of solvent some conformational changes occurs in *COOH and *OCHO (see figure:3.9). For *COOH, Pd-C bond length changes by about 0.04 Å and C-O bond length changes around 0.02 Å. Other bond lengths close to reaction site are also slightly elongated. For *OCHO, O-Pd bond length is stretched about 0.04 Å and O-Pd-O angle changes by about 1°. Other bonds adjacent to it also gets slightly stretched (about 0.02 Å).

Once *OCHO or *COOH has been formed the reaction proceeds further through an electron-proton transfer to form *CO or *HCOOH. For *OCHO it is converted to *HCOOH. However, from *COOH there can be two possible paths. It could either form *CO and H$_2$O or it can lead to formation of *HCOOH. Reaction energetics and its comparison with PANI and change in energetics after including the solvent effect has been discussed further (figure:3.11).

Solvent results in stabilization of the reaction intermediates via non-covalent interactions with solute. Reaction sites for most of them are still on Pd-atom except for *COOH where *COOH binds to N$_4$ nitrogen site and that conformer is 0.02 eV more stable than at the
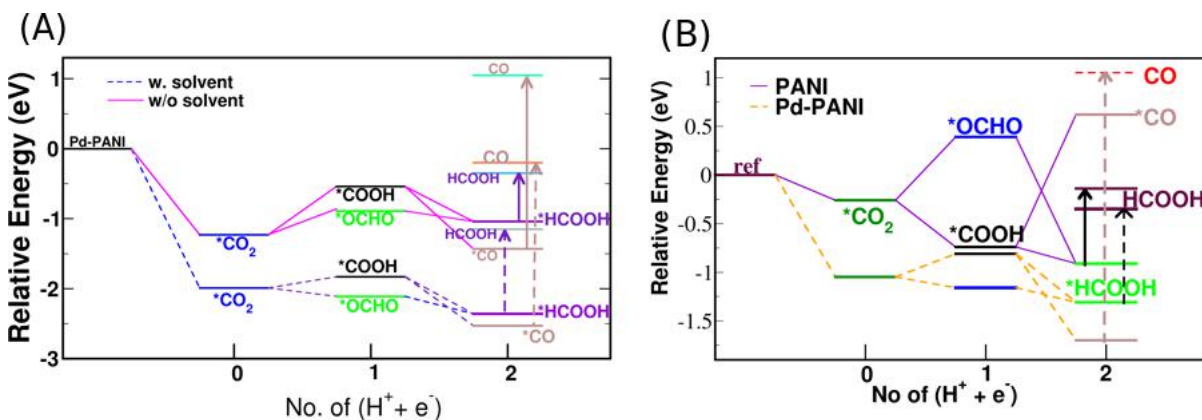
Figure 3.11: (A) Comparison between gas phase energetics and including solvent fro CO_2 to formic acid formation on Pd-PANI. Solvent stabilizes the intermediate but overall does not change energetics patterns. (B) Comparison of energetics for formic acid formation on PANI and Pd-PANI.

Pd-site one (see the appendix table:A.3). The comparison of CO_2 conversion on Pd-PANI with the solvent has been shown in figure:3.11(A). Similar to that of PANI the solvation effect is more where the interaction is strong. Overall reaction energy patterns remain same only energetics goes down.

In PANI we find *COOH is more stable than *OCHO. However, in presence of Pd the stability is reversed (figure: 3.11(B)). *COOH and *OCHO, both the intermediates have sufficient stability on Pd-PANI while on PANI *OCHO is highly unstable. The reaction will proceed mainly through *OCHO on Pd-PANI since it is lower in energy than *COOH. Had the reaction proceeded through *COOH, *CO formation (*COOH $+ H^+ + e^- \rightarrow$ *CO $+$ H_2O) would be more favorable than *HCOOH formation (*COOH $+ H^+ + e^- \rightarrow$ *HCOOH). After formation of *CO, if it does not convert into any other product, it will lead to poisoning the catalytic site of the catalyst due to high desorption energy of *CO (2.47 eV). But there is a chance of *CO to methanol conversion which we will investigate later. The final step is desorption of *HCOOH from the adsorbent. The desorption energy of *HCOOH from Pd-PANI is 0.2 eV more than that from PANI (figure:3.11(B)).

3.4   Interaction of CO and HCOOH with Pd-PANI

Now we will see how CO and HCOOH interacts with Pd-PANI. To understand that first we have looked at HCOOH adsorption on Pd-PANI. HCOOH interacts with Pd-PANI through

C=O bond of HCOOH. The lumo of HCOOH is primarily localized on C=O forming an empty π^* orbital that can accept electrons from Pd atom. Corresponding structure, molecular orbitals projected DOS and integral local DOS has been given in figure:3.12. From charge density difference plot we find that at Pd there is depletion of charge and on C=O there is accumulation of charge (figure:3.12(A)). After interaction C=O bond is elongated by 0.08 Å (1.20 Å to 1.28 Å). C−O is also stretched by around 0.2 Å (1.35 Å to 1.37 Å) resulting in weakening of the C−OH bond. HCOOH also looses its planarity due to change in hybridization from sp^2 to sp^3. To understand what orbitals are involve in hybridization we have also plotted the integral local DOS in the regime of homo-lumo. Here we observed homo-1 and lumo of Pd-PANI-HCOOH have mixed states from Pd-PANI and HCOOH (see figure:3.12(C,E)). However, homo of HCOOH have contribution primarily from PANI (figure:3.12(D)) and very less contribution from Pd states.
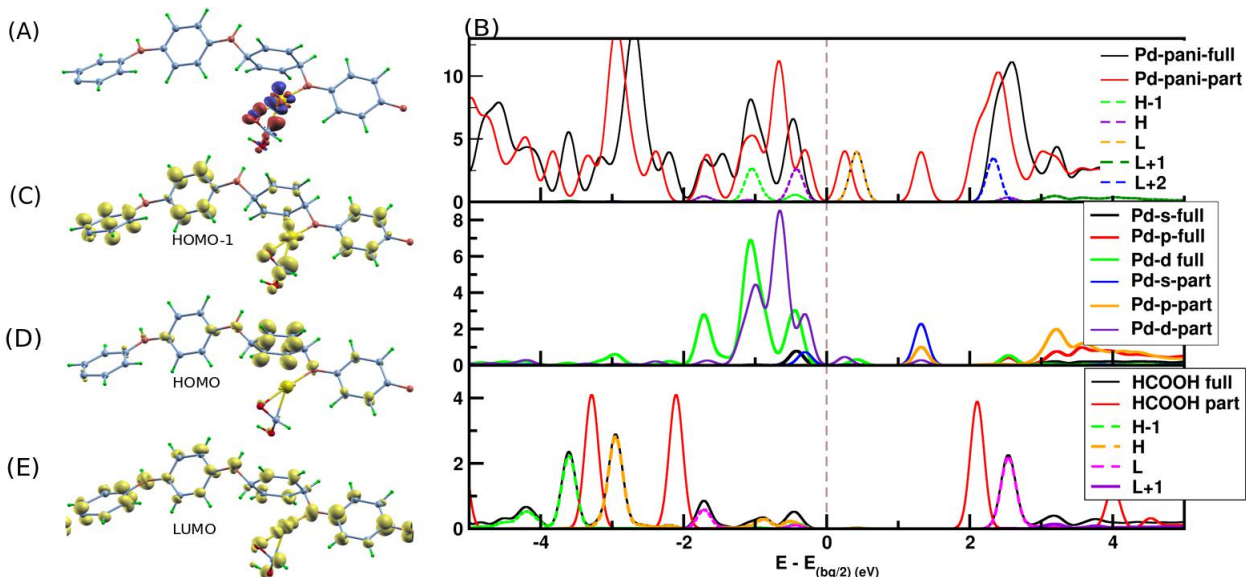
Figure 3.12: (A) Plot of charge density difference isosurface ($\Delta\rho(r) = \rho_{Pd-PANI-HCOOH} - \rho_{Pd-PANI} - \rho_{HCOOH}$). Blue color shows charge depletion and red shows charge accumulation. (B) DOS of HCOOH adsorption on Pd-PANI. Top panel shows the total DOS (black curve) and DOS of Pd-PANI in interacting geometry. The middle panel shows the DOS projected on the Pd-d, s and p states. "full" denotes Pd-PANI-HCOOH and "part" denotes Pd-PANI. The bottom panel shows the DOS Pd-PANI-HCOOH projected on molecular orbitals of HCOOH. H-1, H, L and L+1 denotes the homo-1, homo, lumo and lumo+1 states of HCOOH when it interacts with Pd-PANI. Isosurface of integral local DOS from -1.27 eV to -0.7 eV (C) and -0.7 eV to -0.015 eV (D) and 0.16 eV to 0.67 eV (E) of Pd-PANI-HCOOH (black curve) have been shown.

The interaction of CO with Pd of Pd-PANI occurs through homo, lumo and lumo+1 of CO

(see figure:3.13(B)). Figure:3.13(A) shows charge density difference plot between Pd-PANI-CO, Pd-PANI and CO, which shows a redistribution of charge density takes place. In bottom panel of the figure:3.13(B) we see that homo is getting shifted higher in energy and lumo, lumo+1 shifted towards lower energy with respect to that observed in gas phase. Further, new states are appearing around -1.9 eV and -0.3 eV which mainly comes from the hybridization between CO and Pd of Pd-PANI. Appearance of new states in lumo below zero (-1.8 eV) is a clear signature some charge transfer from Pd to anti-bonding orbital of CO. This can be seen from charge density plot (figure:3.13(A)). We also have plotted the integral local DOS in the regime of homo-lumo. We observed that homo-lumo of Pd-PANI-CO are consist of mixture of CO, Pd and PANI states.
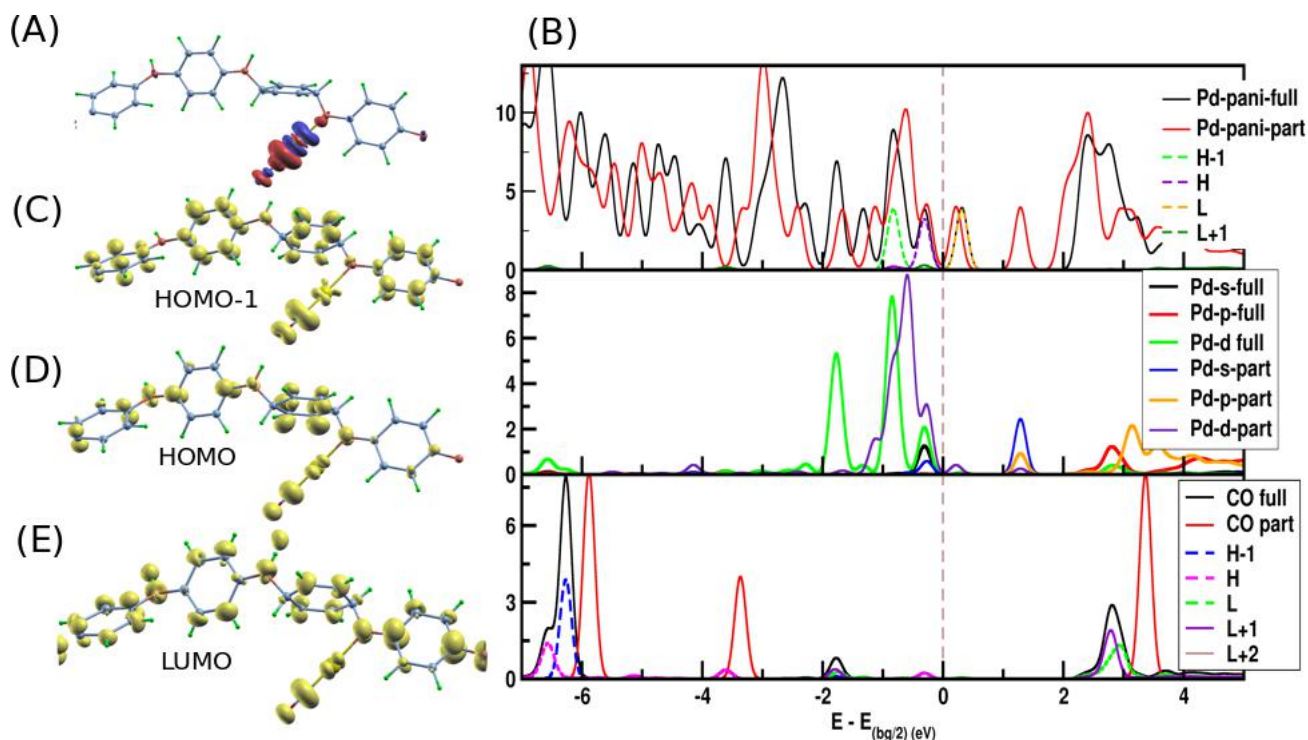
Figure 3.13: (A) Plot of charge density difference isosurface ($\Delta\rho(r) = \rho_{Pd-PANI-CO} - \rho_{Pd-PANI} - \rho_{CO}$). Blue color shows charge depletion and red shows charge accumulation. (B) DOS of CO adsorption on Pd-PANI. Top panel shows the total DOS (black curve) and DOS of Pd-PANI in interacting geometry. The middle panel shows the DOS projected on the Pd-d, s and p states. "full" denotes Pd-PANI-CO and "part" denotes Pd-PANI. The bottom panel shows the DOS Pd-PANI-CO projected on molecular orbitals of CO. H-1, H, L and L+1 denotes the homo-1, homo, lumo and lumo+1 states of CO when it interacts with Pd-PANI. Integral local DOS from -1.12 eV to -0.49 eV (C), -0.49 eV to -0.04 eV (D) and from 0.07 eV to 0.56 eV (E) of Pd-PANI-CO (black curve in the first panel of B).

3.5   Reduction of CO$_2$ to MeOH

MeOH can be formed in two different ways in ERC. One is the reduction of formic acid and the other one through the reduction of CO. We have investigated both. For methanol formation, the crucial intermediate step is either *CO or *HCOOH. Furthermore, one electron-proton transfer takes place and *CO will form *COH or *CHO. However, *HCOOH will only form *CHO + H$_2$O via taking electron-proton. The possible mechanistic path for methanol formation has been discussed earlier (figure:3.2(B)).
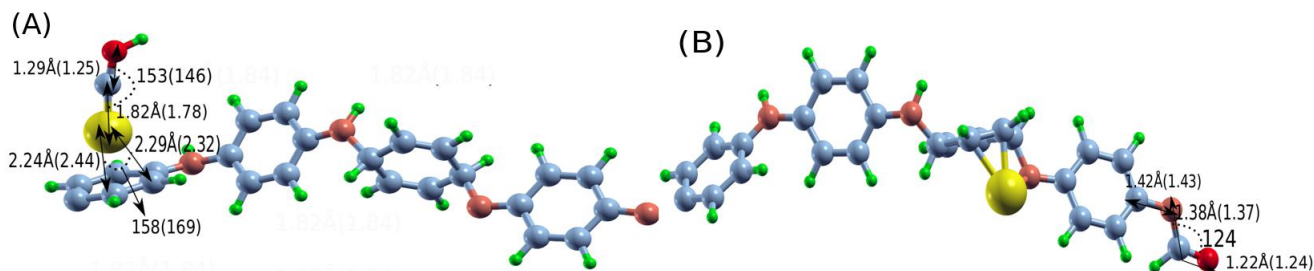
Figure 3.14: Most stable conformer of *COH (A) and *CHO (B) has been shown. Conformational changes after including solvent effect also have been shown. The values within parenthesis are in solvent.

Optimized geometries of the most stable conformer of *COH and *CHO along with their conformational changes after including the solvent effect also have been shown (figure:3.14). For *COH, in gas phase Pd is atop the C-C double bond of the benzene ring. However, after including solvent effect the Pd atom slightly shifted towards hollow site of the benzene ring Pd-C (C=C of benzene ring) bonds are elongated by about 0.2 Åand C-Pd-C angle also stretched by about 11°. Pd-C bond (C of COH) reduced about 0.04 Å. Other bond lengths and bond angles adjacent to it also gets slightly affected in presence of solvent. For *CHO change in bond length and bond angle is not very significant. One more important thing we have observed here which is change in the reaction site while moving from one intermediate to other. We had not observed change in reaction site for formic acid formation except for *COOH intermediate. In this case reaction site changes from Pd atom to N$_4$ nitrogen after including the solvent effect. This change in reaction site could be barrier less or can cost some additional energy. This energy barrier we have not considered in the present work.

After forming *CHO or *COH again a electron-proton transfer occurs and it can form either *CHOH or *CH$_2$O. Most stable conformer of *CH$_2$O (figure:3.15(A)) and *CHOH (figure:3.15(B)) and respective conformational changes after including solvent correction have been shown in the figure:3.15. Change in reactive site has been observed for bothe the in-
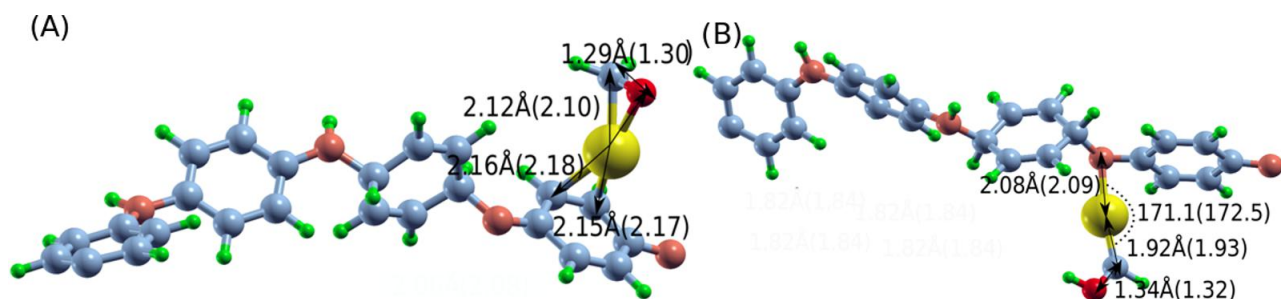
Figure 3.15: Most stable conformer of *CH$_2$O (A) and *CHOH (B) has been shown. Conformational changes after including solvent effect also have been shown. The values within parenthesis are in solvent.

termediates. For *CH$_2$O, Pd-C bonds (C=C carbons of PANI which are attached to Pd) are elongated by about 0.02 Å as compared to gas phase bond length and Pd-C with C of *CH$_2$O is also stretched by the same amount. Bond angle does not change significantly. For *CHOH, bonds connected with Pd is stretched by about 0.01 Å and a slight change in angle (with respect to their gas phase) has been observed after including the solvent effect. Change in reactive site has been observed for both the intermediates.
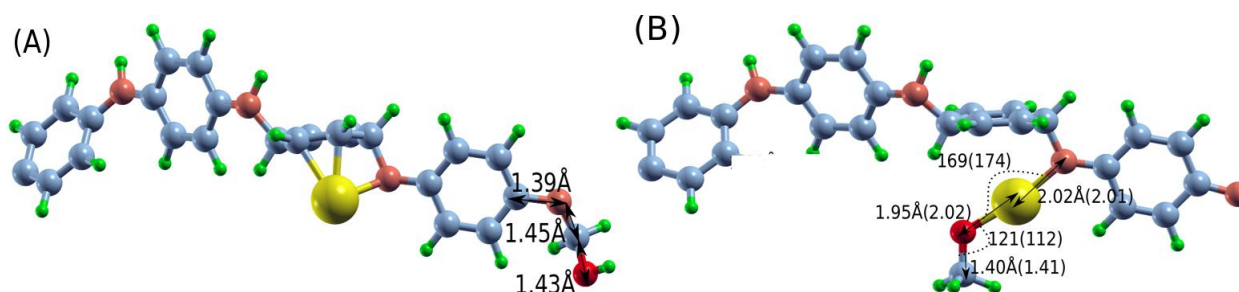
Figure 3.16: Most stable conformer of *CH$_2$OH (A) and *CH$_3$O (B) has been shown. Conformational changes after including solvent effect also have been shown. The values within parenthesis are in solvent.

Now after *CH$_2$O or *CHOH has been formed, and by taking a proton-electron leads to formation of either *CH$_2$OH or CH$_3$O. Most stable conformer of *CH$_2$OH (figure:3.16(A)) and *CH$_3$O (figure:3.16(B)) and the respective changes after including solvent effect have been shown in figure:3.16. For *CH$_2$OH no significant change appears in either in bond length and bond angle after including the solvent effect. However, for *CH$_3$O though the bond length does not change much, O-Pd-N angle is stretched by about 5° and Pd-O-C angle is shrinked by about 9°. After forming *CH$_3$O or *CH$_2$OH by taking a proton and electron it will lead to the formation of *CH$_3$OH. Here also we observed change in reactive sites. Most stable conformer of MeOH and corresponding changes after including the solvent effect have
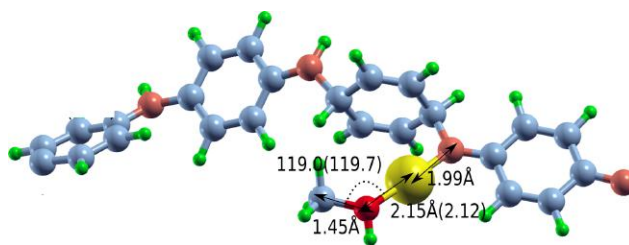
Figure 3.17: Most stable conformer of CH$_3$OH has been shown. Conformational changes after including solvent effect also have been shown. The values within parenthesis are in solvent.

been shown in the figure:3.17. O-Pd bond length changes about 0.03 Å with respect to gas phase bond length.

So far we have looked at all the intermediates and their most stable configuration for methanol formation and effect of solvent on their geometries. Now we will report the relative stability of the reaction intermediates (figure:3.18). We have already discussed the formation of *HCOOH or *CO on Pd-PANI (subsection:3.3). So now the next step is the formation of *COH or *CHO from *CO by accepting a proton and electron. Formation of *COH and *CHO both are uphill but *COH is thermodynamically unfavorable. This is because COH is highly unstable due to the fact that the carbon is having three unpaired electrons and it can not be stabilized enough through the interaction with only one Pd-atom. So in most cases hydrogen is detached from COH and it goes back to CO (see appendix table:A.12). In contrast, CHO has only one unpaired electron which can be stabilized through the interaction with Pd-atom. Again through an electron-proton transfer *CHO gets converted into either *CHOH or *CH$_2$O because proton can be accepted by either carbon or oxygen. We find that *CH$_2$O formation is more favorable than *CHOH. *CH$_2$O is more appropriate to form because it can interact with Pd by C=O of *CH$_2$O. However, *CHOH will interact through C of *CHOH and Pd atom. One more electron-proton transfer and either of them can be converted into *CH$_3$O or *CH$_2$OH. Thermodynamically *CH$_2$OH is more preferable due to strong bonding between C-Pd in *CH$_2$OH then O-Pd in *CH$_3$O. After taking a proton and electron either of them (*CH$_3$O or *CH$_2$OH) will leads to the formation of *CH$_3$OH and finally it will desorbed from Pd-PANI.

After including the effect of solvent similar effect have been observed as in case of HCOOH formation. Metastable states gets stabilized significantly but over all reaction energetics does not change. Desorption energy of *CO increases about 0.25 eV (with respect to gas phase). So now gas phase CO formation is much more difficult than the genesis of MeOH due to high
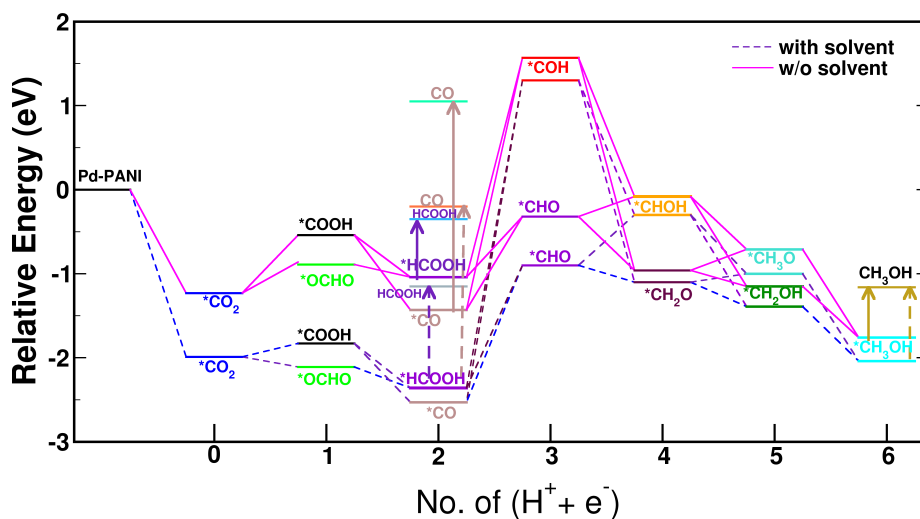
Figure 3.18: Relative energy plot for complete reaction pathway. For gas phase energies are rescaled by the energy of Pd-PANI+CO_2+3H_2 and for solvent case these are rescaled by Pd-PANI (env.)+CO_2 +3H_2.

desorption energy.

3.6 Conclusion

From our calculations we find that the possible path for formic acid formation primarily goes through *OCHO intermediate on PANI:

$$^*CO_2 \rightarrow^* COOH \rightarrow^* HCOOH$$

However, when we use Pd-PANI as a catalyst reaction goes through *OCHO intermediate:

$$^*CO_2 \rightarrow^* OCHO \rightarrow^* HCOOH$$

Formation of MeOH occurs through *COOH intermediate on Pd-PANI.

$$^*CO_2 \rightarrow^* COOH \rightarrow^* CO \rightarrow^* CHO \rightarrow^* CH_2O \rightarrow^* CH_2OH \rightarrow^* CH_3OH$$
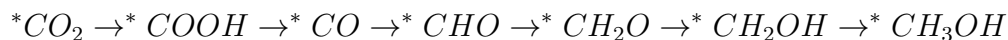
In the experiment Weiran Zheng *et al.* had not observed any genesis of MeOH on PANI due to no formation of *CO occurs at PANI, which is a crucial intermediate for MeOH formation. They have not observed any methanol formation till -0.5 eV external potential because genesis of methanol occurs through *CO reduction which is an uphill path (figure:3.11) and requires

37

some energy cost to make this path thermodynamically favorable. Furthermore, they had observed formic acid formation was almost three times higher than methanol formation. From our calculations we see that this happens primarily for two reasons: (a) HCOOH formed through *OCHO while methanol formation occurs primarily through *COOH whose formation in presence of Pd-PANI is thermodynamically unfavorable. (b) Uphill path for methanol formation. Furthermore, MeOH formation from *HCOOH requires more energy cost than HCOOH desorption from catalyst. When we use Pd-PANI as a catalyst, formation of *CO is more fauvarable than *HCOOH from *COOH intermediate. Furthermore, desorption of CO requires more energy than to reduce it. So no CO has been observed in gas phase. However, when we increase the external potential (-1.1 eV), CO desorption also becomes thermodynamically favorable. So trace amount of CO has been observed in gas phase at -1.1.eV.

Chapter 4

Future Directions

S o far we have studied the reduction of CO_2 to HCOOH and CH_3OH by PANI and Pd-PANI by considering a simple model system. Further our calculations do not include finite temperature and entropic effects that might be important for these systems. Additionally we also do not consider the effects of external potential and pH on the reaction energetics. Hence as a future outlook to this problem we can include the above mentioned complexities. This will help us not only to model a realistic system but also provide insight as to how these terms affect the energetics. Below we briefly explain how these can be incorporated.

4.1   Effect of external potential and pH

Applied external potential increase the current efficiency of the product formation. In this study we have not included the external potential effect on reaction energetics. We are not able to explain some of the experimental observation such as why methanol does not forms till -0.5 eV potential or why methanol formation decreases after -0.9 eV. To answer such question we need to incude the effect of external potential. This effect can be included in free energy diagrams with the Nernst equation $\Delta G = -nFE$, where n is number of electron, F is Faraday constant and E is the applied potential. To calculate ΔG in eV we can write this equation as $\Delta G = -nE$.

Experimental reaction conditions are different than pH=0. So it will be good to consider the pH effect. To model the consequence of pH in free energy is not a trivial task. The simplest way to take into account the pH effect is from gibb's free energy equation given by Nørskov[29] $G_{pH} = -kT \ln[H^+]$, where $[H^+]$ is the concentration of H^+ ions.

4.2 Zero point energy and entropy correction

To explain the more realistic free energy pathways we need to include the zero point energy (ZPE) correction and vibrational entropy. The assumption we make here that the polymeric chain and adsorbed species does not have significant contribution form rotational and translational entropy due to strongly covalent binded complex. So it does not have high flexibility for rotational or translational motion. So we will consider only ZPE and vibrational entropy correction. We can also include the temperature dependence also.

4.3 More refined model

In this study we have taken a very simplistic model to explain the experimental observation like modeling PANI we have taken only four rings in unit cell and for Pd cluster we have taken a Pd-adatom on PANI. If we increase the number of rings in unit cell the coiling in the chain will be different, dihedral angle among the rings will change and this effect could alter energetics and interaction significantly. Furthermore, we have taken only one string of polymeric chain. However, in the real scenario there will be some $\pi - \pi$ stacking between the strings. So we also can include this complexity in the system. Also the reaction can be influenced by the size of the Pd cluster. To get more refined minimum energy configurations we can also use molecular dynamics (MD) simulations. Moreover sometimes explicit solvent model needs to be incorporated.

4.4 Change in active site

From our calculations, in some cases, we have observed the change in reaction site while going from one intermediate to another. This change in reactive site may also involve some additional energy barrier. Having an idea about the required energy cost will give better understanding about the reaction energetics. To calculate the required additional energy for the change in reaction site we can do climbing image nudged elastic band (CI-NEB) calculation. To know the actual insight about the reaction energetics this effect also needs to be included. We also need to understand what are the driving forces for change in the reactive sites.

Appendix A

Possible conformers for different intermediates

Hᴇʀᴇ we present all the conformer which we have tried for different intermediates with there relative stability with respect to most stable ones. Values shows in black represent gas phase relative energies and in red represent relative energies in presence of solvent. All the energies are in eV.
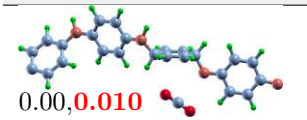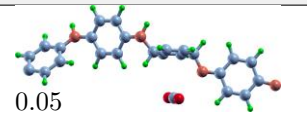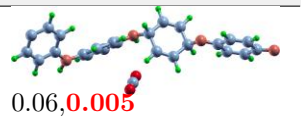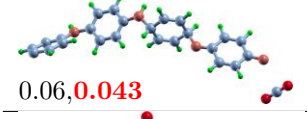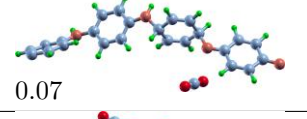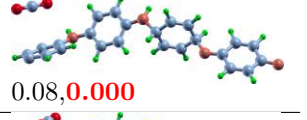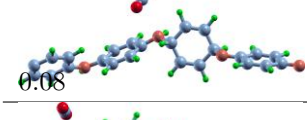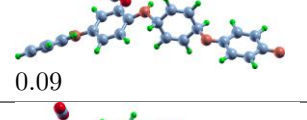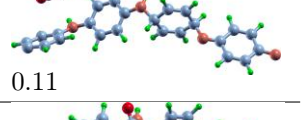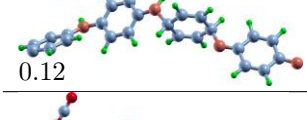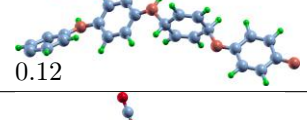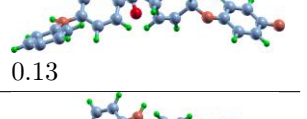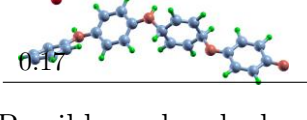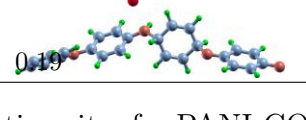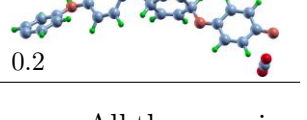
CO2 adsorption on PANI Optimized Geometries		
0.00,**0.010**	0.05	0.06,**0.005**
0.06,**0.043**	0.07	0.08,**0.000**
0.08	0.09	0.11
0.12	0.12	0.13
0.17	0.19	0.2

Table A.1: Possible explored adsorption sites for PANI-CO$_2$ case. All the energies are rescaled w.r.t most stable configuration among them.
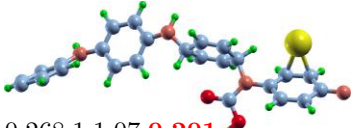
Table A.2: Possible explored adsorption sites for PANI-OCHO case. All the energies are rescaled w.r.t most stable configuration among them.
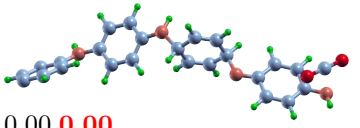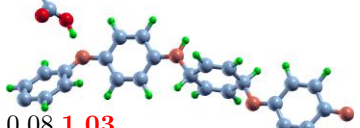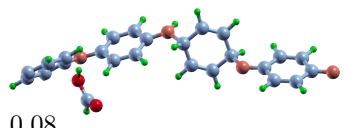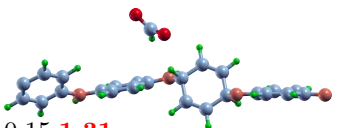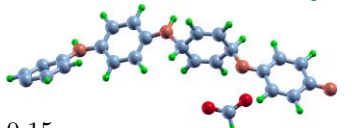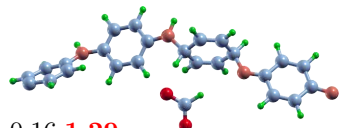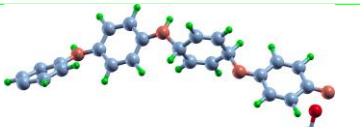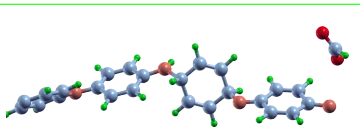
OCHO interaction with PANI Optimized Geometries		
0.00,**0.00**	0.08,**1.03**	0.08
0.15,**1.31**	0.15	0.16,**1.29**
0.16	0.16,**1.32**	

Table A.3: Possible explored adsorption sites for PANI-COOH case. All the energies are rescaled w.r.t most stable configuration among them. All the energies are in eV.
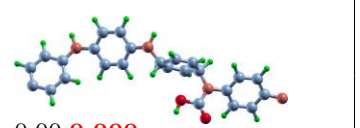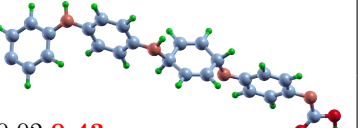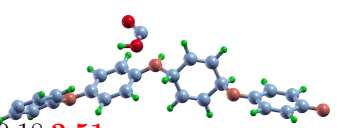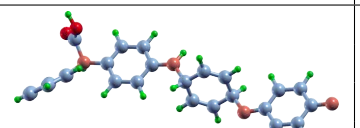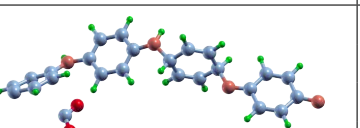
COOH interaction with PANI Optimized Geometries		
0.00,**0.000**	0.02,**0.43**	0.18,**2.51**
0.19	0.19,**2.57**	

Table A.4: Possible explored adsorption sites for PANI-CO case. All the energies are rescaled w.r.t most stable configuration among them.
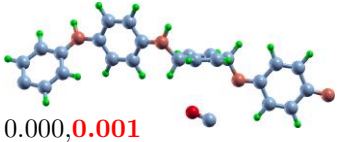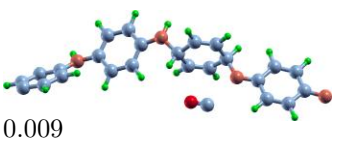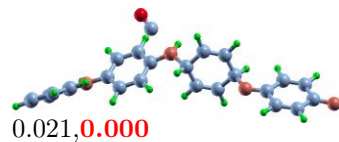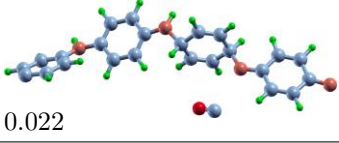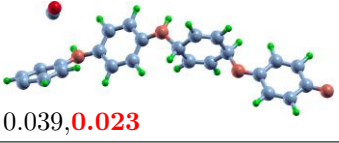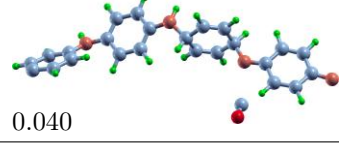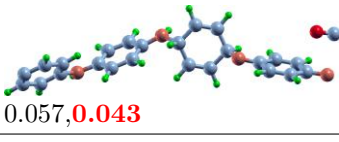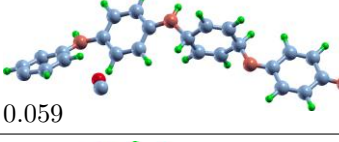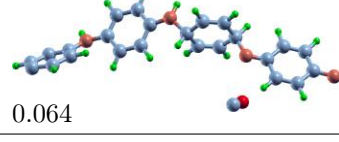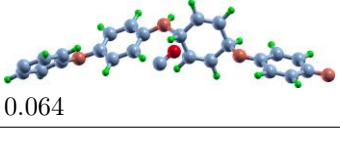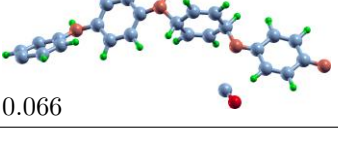
Table A.5: Possible explored adsorption sites for PANI-HCOOH case. All the energies are rescaled w.r.t most stable configuration among them.
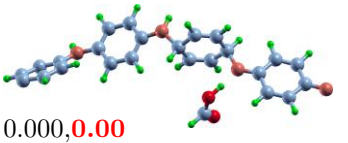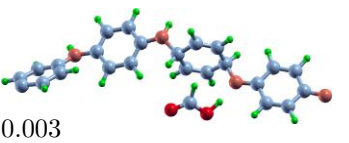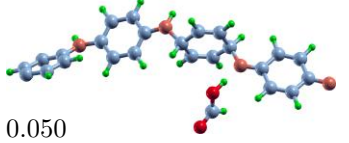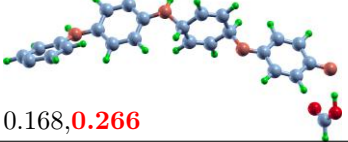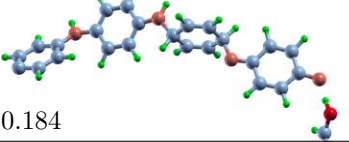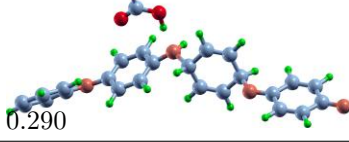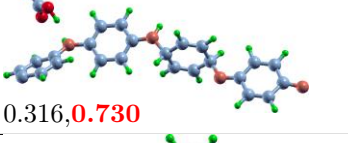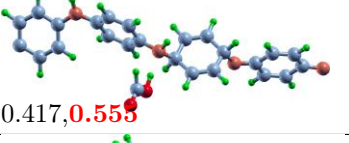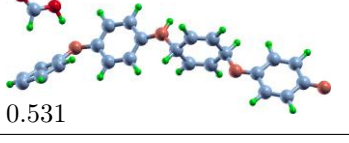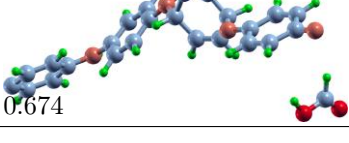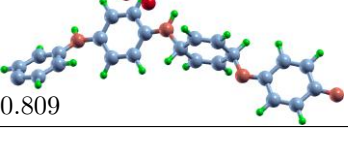
Table A.6: Possible explored adsorption sites for Pd-PANI case. All the energies are rescaled w.r.t most stable configuration among them.

Pd interaction on PANI Optimized Geometries		
0.000,**0.000**	0.269,**0.104**	0.355,**0.355**
0.462,**0.299**	0.472	0.520,**0.398**
0.539	0.548	0.574
0.716	1.033	1.178

Table A.7: Possible explored adsorption sites for Pd-PANI-CO2 case. All the energies are rescaled w.r.t most stable configuration among them.
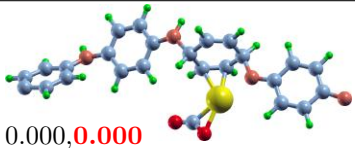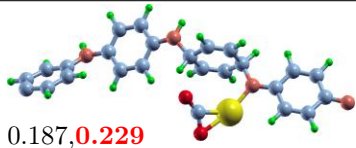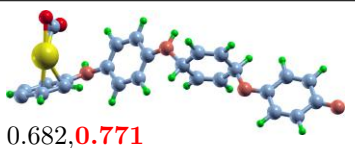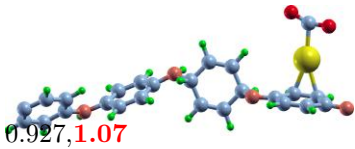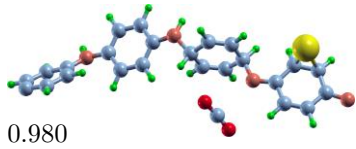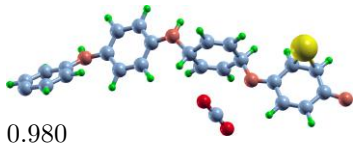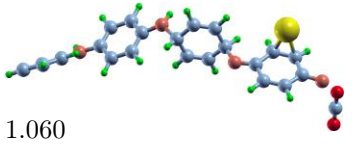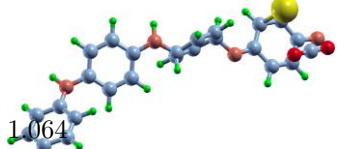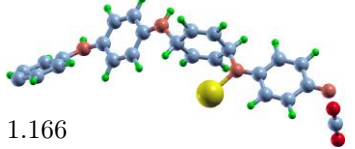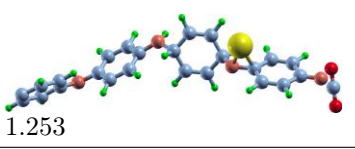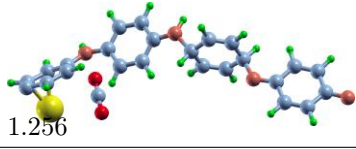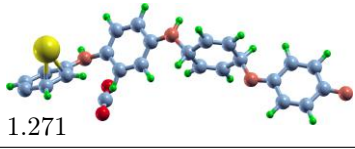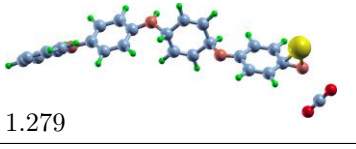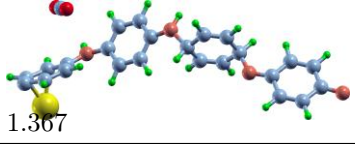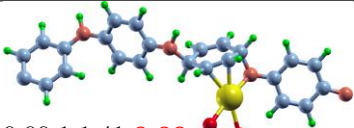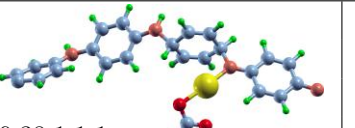
CO2 adsorption on Pd-PANI		
Optimized Geometries		
0.000,**0.000**	0.187,**0.229**	0.682,**0.771**
0.927,**1.07**	0.980	0.980
1.060	1.064	1.166
1.253	1.256	1.271
1.279	1.303,**1.31**	1.367

Table A.8: Possible explored adsorption sites for Pd-PANI-COOH case. All the energies are rescaled w.r.t most stable configuration among them.
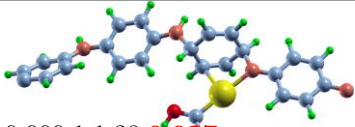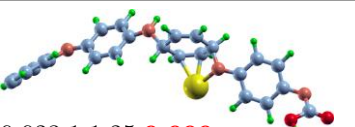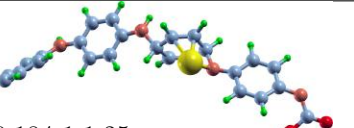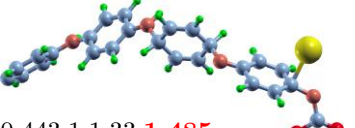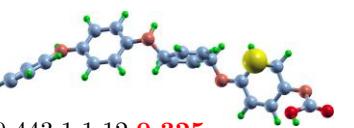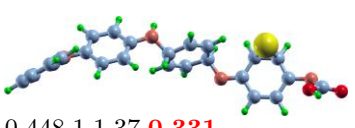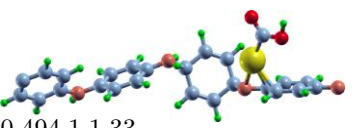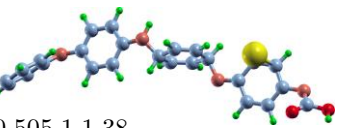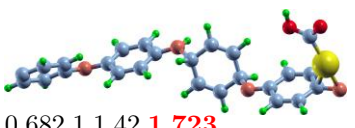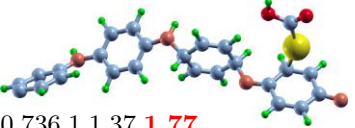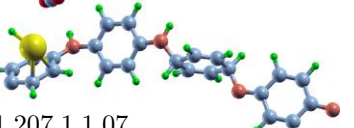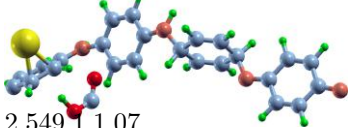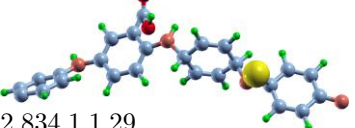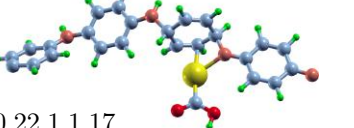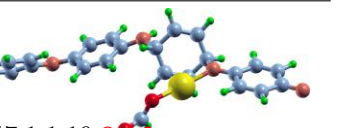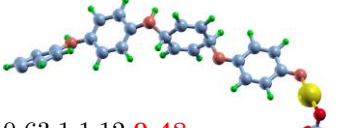

COOH interaction with Pd-PANI Optimized Geometries		
0.000,1,1.38,**0.027**	0.023,1,1.25,**0.000**	0.184,,1,1.25
0.268,1,1.07,**0.201**	0.443,1,1.33,**1.485**	0.443,1,1.12,**0.325**
0.448,1,1.37,**0.331**	0.494,1,1.33	0.505,1,1.38
0.682,1,1.42,**1.723**	0.736,1,1.37,**1.77**	1.207,1,1.07
2.549,1,1.07	2.834,1,1.29	0.22,1,1.17

Table A.9: Possible explored adsorption sites for Pd-PANI-OCHO case. All the energies are rescaled w.r.t most stable configuration among them.
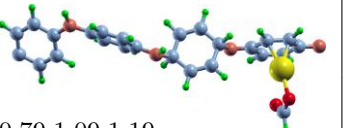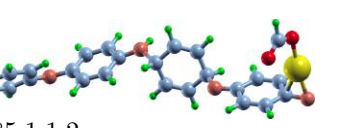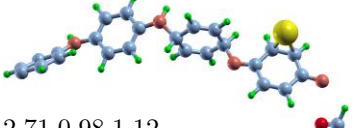
OCHO interaction with Pd-PANI Optimized Geometries		
0.00,1,1.41,**0.00**	0.38,1,1.1	0.47,1,1.19,**0.16**
0.63,1,1.12,**0.48**	0.79,1.09,1.19	0.85,1,1.2
2.71,0.98,1.12		

Table A.10: Possible explored adsorption sites for Pd-PANI-CO case. All the energies are rescaled w.r.t most stable configuration among them.

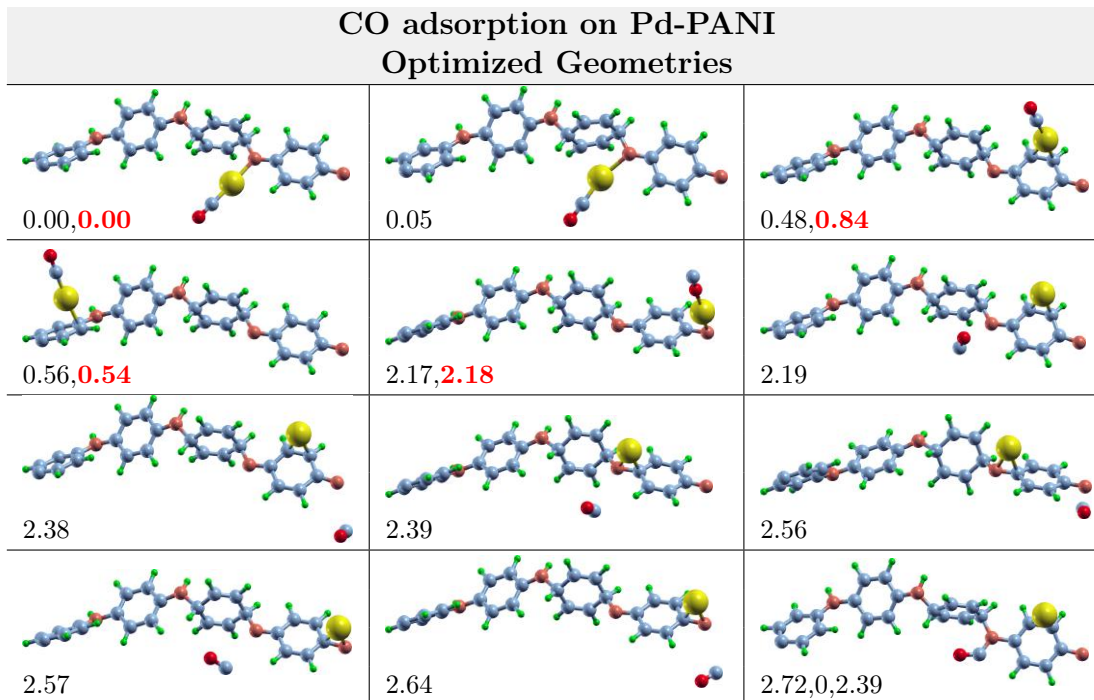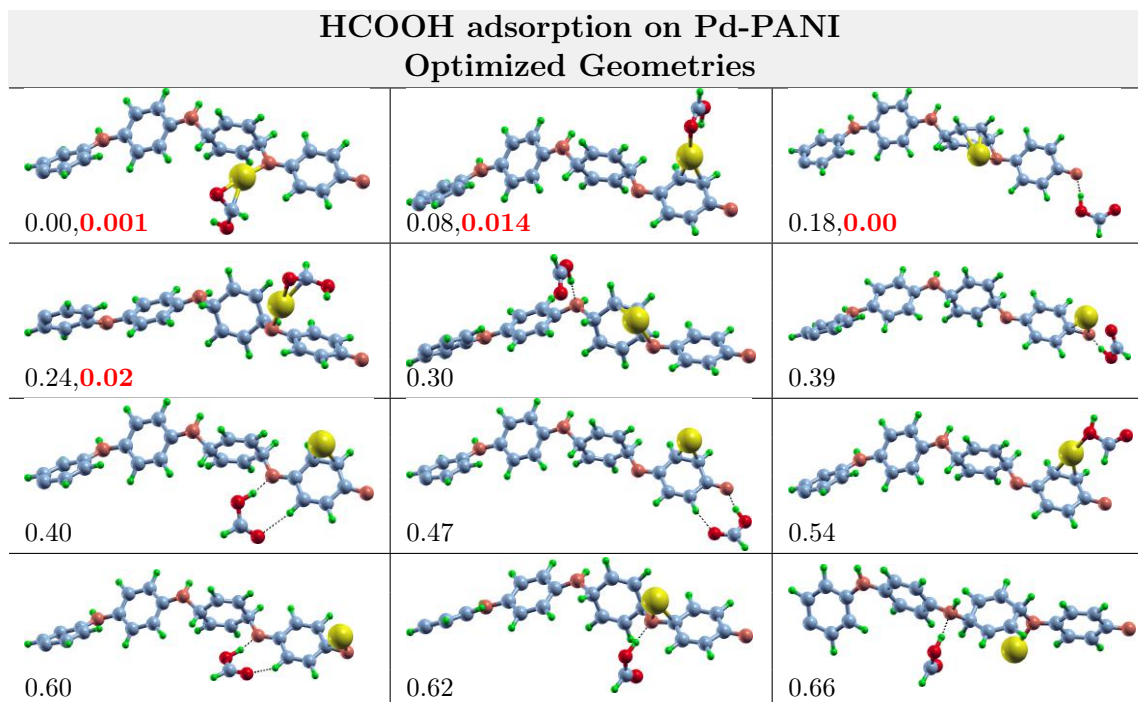| CO adsorption on Pd-PANI Optimized Geometries		
0.00,**0.00**	0.05	0.48,**0.84**
0.56,**0.54**	2.17,**2.18**	2.19
2.38	2.39	2.56
2.57	2.64	2.72,0,2.39

Table A.11: Possible explored adsorption sites for Pd-PANI-HCOOH case. All the energies are rescaled w.r.t most stable configuration among them.

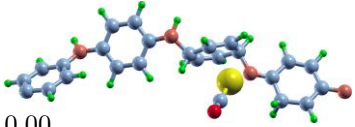

HCOOH adsorption on Pd-PANI Optimized Geometries		
0.00,**0.001**	0.08,**0.014**	0.18,**0.00**
0.24,**0.02**	0.30	0.39
0.40	0.47	0.54
0.60	0.62	0.66

Table A.12: Possible explored adsorption sites for Pd-PANI-COH case. All the energies are rescaled w.r.t most stable configuration among them.
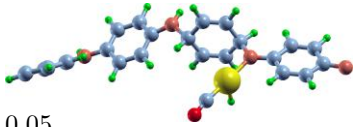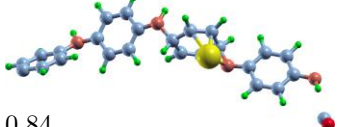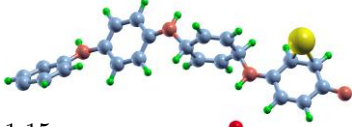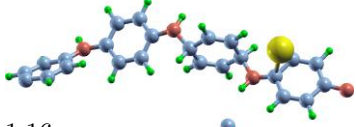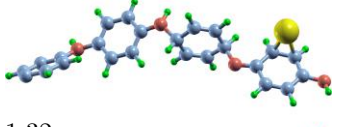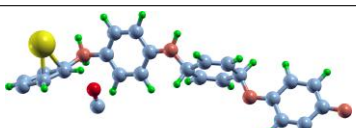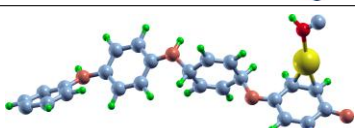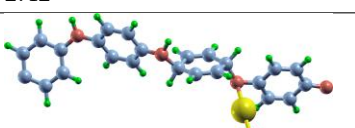
COH interaction with Pd-PANI Optimized Geometries		
0.00	0.05	0.84
1.15	1.16	1.32
2.42	3.23	4.30
4.44		

Table A.13: Possible explored adsorption sites for Pd-PANI-CHO case. All the energies are rescaled w.r.t most stable configuration among them.
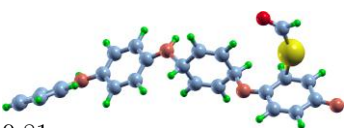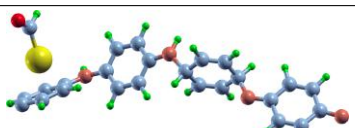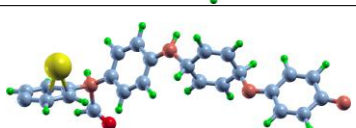
CHO interaction with Pd-PANI Optimized Geometries		
0.00	0.39	0.42
0.48	0.50	0.81
0.94	2.85	

Table A.14: Possible explored adsorption sites for Pd-PANI-CHOH case. All the energies are rescaled w.r.t most stable configuration among them.

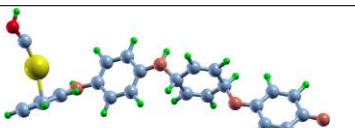| CHOH interaction with Pd-PANI Optimized Geometries		
0.00	0.09	0.12
0.14	0.32	0.35
0.39	0.67	
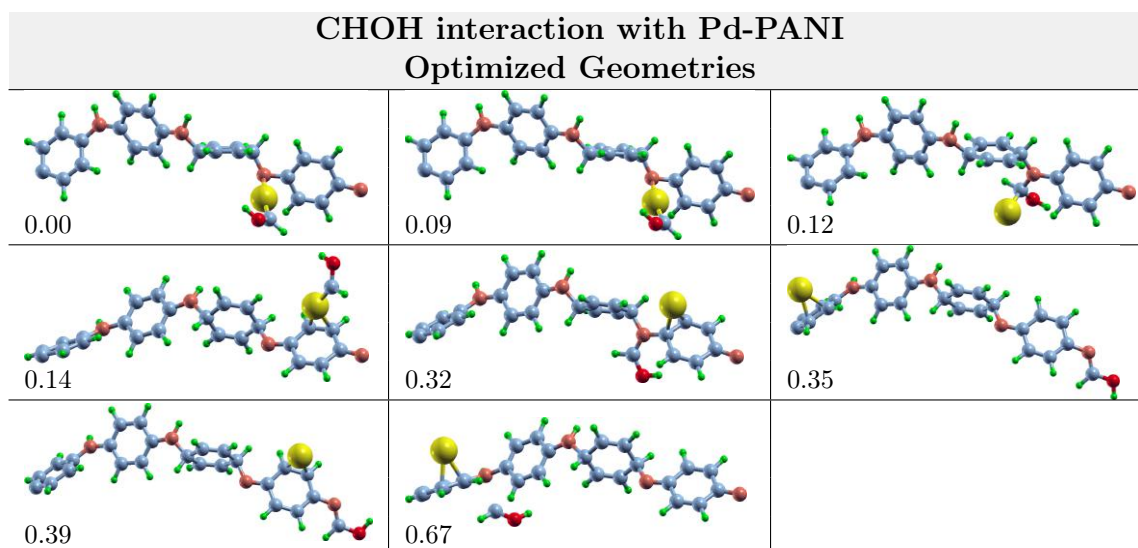
Table A.15: Possible explored adsorption sites for Pd-PANI-CH2O case. All the energies are rescaled w.r.t most stable configuration among them.

CH2O interaction with Pd-PANI Optimized Geometries		
0.00	0.17	0.20
1.22	1.38	

Table A.16: Possible explored adsorption sites for Pd-PANI-CH3O case. All the energies are rescaled w.r.t most stable configuration among them.
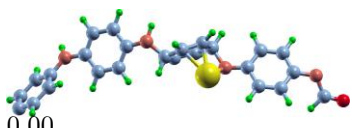
CH3O interaction with Pd-PANI Optimized Geometries		
0.00	0.33	0.50
1.99	2.39	2.61

Table A.17: Possible explored adsorption sites for Pd-PANI-CH2OH case. All the energies are rescaled w.r.t most stable configuration among them.
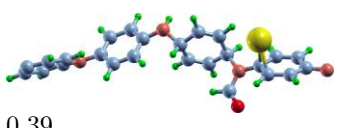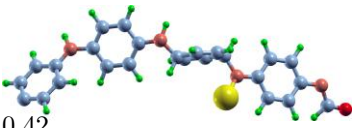
CH2OH interaction with Pd-PANI Optimized Geometries		
0.00	0.05	0.13
0.30	0.36	0.54
0.64	2.14	

Table A.18: Possible explored adsorption sites for Pd-PANI-Methanol case. All the energies are rescaled w.r.t most stable configuration among them.
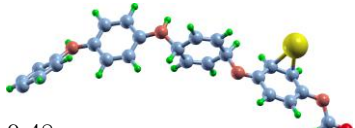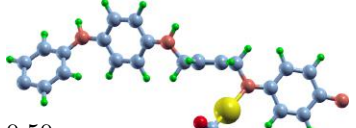
Methanol adsorption Optimized Geometries		
0.00	0.09	0.09
0.17	0.22	0.39
0.39	0.46	0.49
0.57	0.66	0.73
0.83		

Bibliography

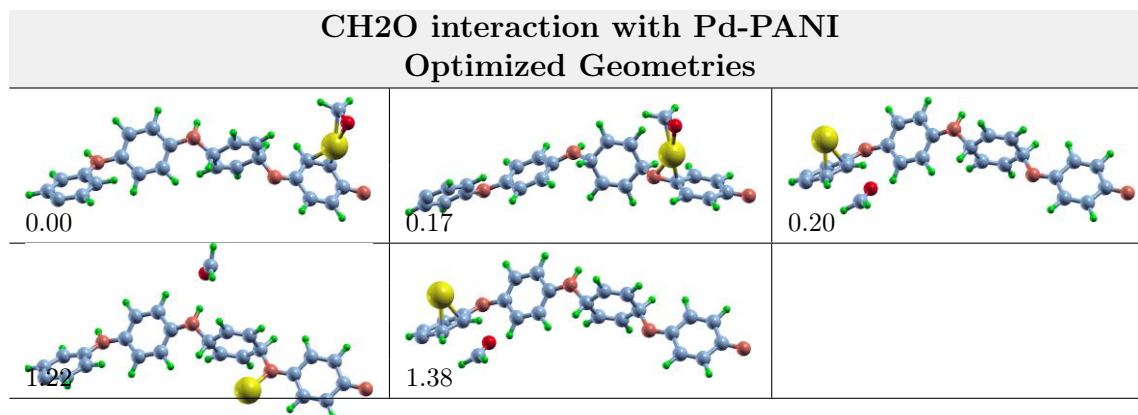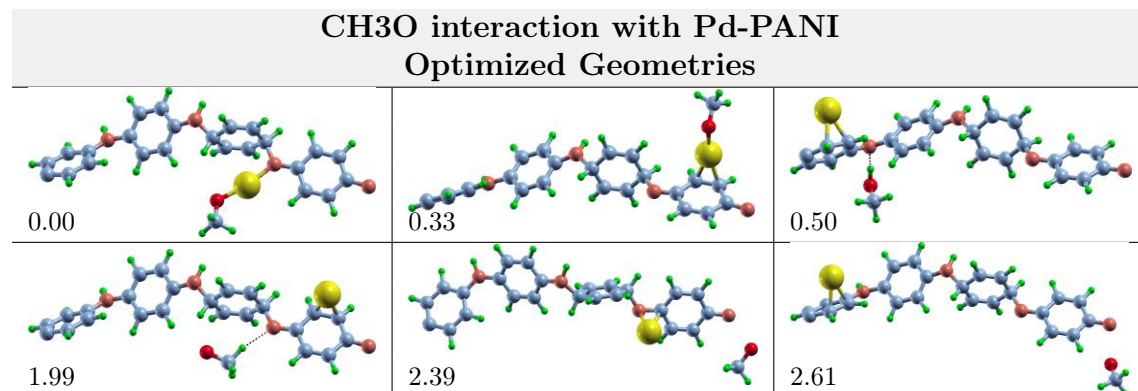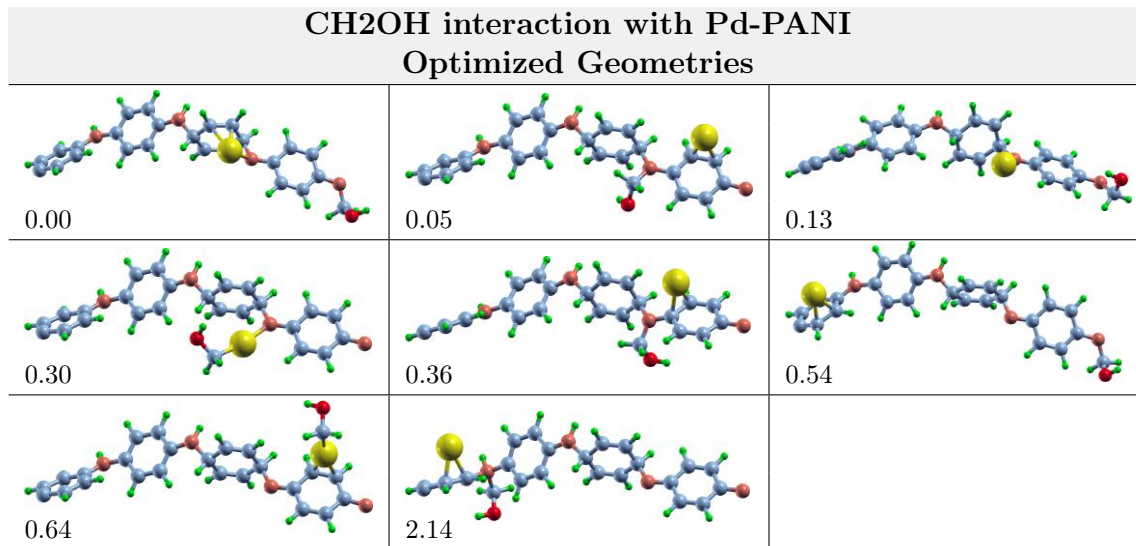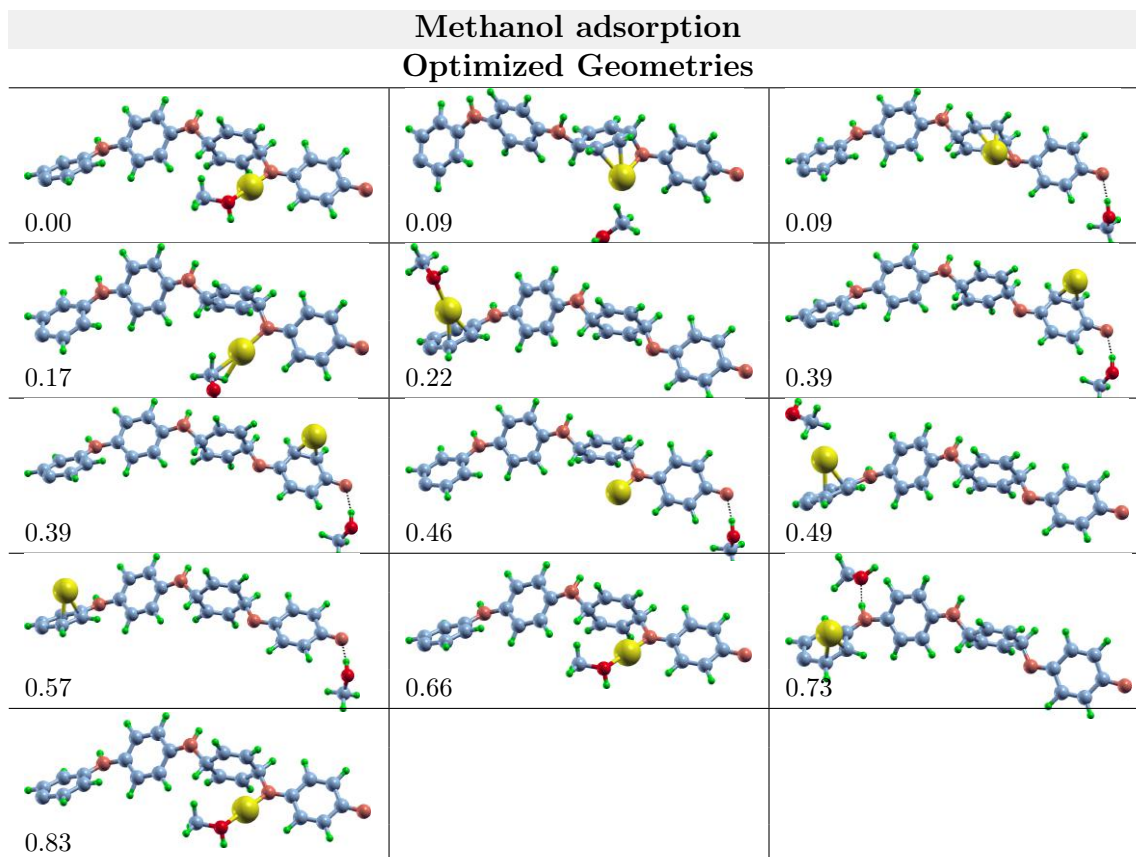[1] J. Albo, M. Alvarez-Guerra, P. Castano, and A. Irabien. Towards the electrochemical conversion of carbon dioxide into methanol. *Green Chem.*, 17:2304–2324, 2015.

[2] R. Socolow and S. Pacala. *Science*, 305:968, 2004.

[3] C. S. Song. *Catal. Today*, 115:2, 2006.

[4] Wenzhen Li. *Electrocatalytic Reduction of carbon dioxide to Small Organic Molecule Fuels on Metal Catalysts*, chapter 5, pages 55–76.

[5] Chen Xu Zhao, Yi Fan Bu, Wang Gao, and Qing Jiang. Carbon dioxide reduction mechanism on the Pb(111) surface: Effect of solvent and cations. *The Journal of Physical Chemistry C*, 121(36):19767–19773, 2017.

[6] Jinli Qiao, Yuyu Liu, Feng Hong, and Jiujun Zhang. A review of catalysts for the electroreduction of carbon dioxide to produce low-carbon fuels. *Chem. Soc. Rev.*, 43:631–675, 2014.

[7] Mar Pérez-Fortes, Jan C. Schöneberger, Aikaterini Boulamanti, Gillian Harrison, and Evangelos Tzimas. Formic acid synthesis using CO2 as raw material: Techno-economic and environmental evaluation and market potential. *International Journal of Hydrogen Energy*, 41(37):16444 – 16462, 2016. Special Issue: Hydrogen and Fuel Cell Developments: A special issue on the 8th International Conference on Sustainable Energy and Environmental Protection (SEEP 2015), 11–14 August 2015, Paisley, Scotland, UK.

[8] Mar Pérez-Fortes, Jan C. Schöneberger, Aikaterini Boulamanti, and Evangelos Tzimas. Methanol synthesis using captured CO2 as raw material: Techno-economic and environmental assessment. *Applied Energy*, 161:718 – 732, 2016.

[9] Weiran Zheng, Simantini Nayak, Weizi Yuan, Zhiyan Zeng, Xinlin Hong, Kylie A. Vincent, and Shik Chi Edman Tsang. A tunable metal-polyaniline interface for efficient carbon dioxide electro-reduction to formic acid and methanol in aqueous solution. *Chem. Commun.*, 52:13901–13904, 2016.

[10] Weiran Zheng, Ho Wing Man, Lin Ye, and Shik Chi Edman Tsang. Electroreduction of carbon dioxide to formic acid and methanol over a palladium/polyaniline catalyst in acidic solution: A study of the palladium size effect. *Energy Technology*, 5(6):937–944, 2017.

[11] J.M Thijssen. *Computational Physics*. 2013.

[12] W. Holthausen, C.M.; Koch. *A Chemist's Guide to Density Functional Theory.* 2000.

[13] Frank Jensen. *Introduction to Computational Chemistry.* John Wiley & Sons, 2006.

[14] M. C. Payne, M. P. Teter, D. C. Allan, T. A. Arias, and J. D. Joannopoulos. Iterative minimization techniques for ab initio total-energy calculations: molecular dynamics and conjugate gradients. *Rev. Mod. Phys.*, 64:1045–1097, Oct 1992.

[15] P. Hohenberg and W. Kohn. Inhomogeneous electron gas. *Phys. Rev.*, 136:B864–B871, Nov 1964.

[16] W. Kohn and L. J. Sham. Self-consistent equations including exchange and correlation effects. *Phys. Rev.*, 140:A1133–A1138, Nov 1965.

[17] Richard M. Martin. *Electronic Structure: Basic Theory and Practical Methods.* Cambridge University Press, 2004.

[18] David S. Sholl and Janice A. Steckel. *Nuts and Bolts of DFT Calculations.* John Wiley Sons, Inc., 2009.

[19] Oliviero Andreussi, Ismaila Dabo, and Nicola Marzari. Revised self-consistent continuum solvation in electronic-structure calculations. *The Journal of Chemical Physics*, 136(6):064102, 2012.

[20] Paolo Giannozzi, Stefano Baroni, Nicola Bonini, Matteo Calandra, Roberto Car, Carlo Cavazzoni, Davide Ceresoli, Guido L Chiarotti, Matteo Cococcioni, Ismaila Dabo, Andrea Dal Corso, Stefano de Gironcoli, Stefano Fabris, Guido Fratesi, Ralph Gebauer, Uwe Gerstmann, Christos Gougoussis, Anton Kokalj, Michele Lazzeri, Layla Martin-Samos, Nicola Marzari, Francesco Mauri, Riccardo Mazzarello, Stefano Paolini, Alfredo Pasquarello, Lorenzo Paulatto, Carlo Sbraccia, Sandro Scandolo, Gabriele Sclauzero, Ari P Seitsonen, Alexander Smogunov, Paolo Umari, and Renata M Wentzcovitch. Quantum espresso: a modular and open-source software project for quantum simulations of materials. *Journal of Physics: Condensed Matter*, 21(39):395502 (19pp), 2009.

[21] J. P. Perdew, K. Burke, and M Ernzerhof. Generalized gradient approximation made simple. *Phys. Rev. Lett.*, 77:3865, 1996.

[22] H. J. Monkhorst and J. D Pack. Special points for brillonin-zone integrations. *Phys. Rev. B: Solid State*, 13:5188, 1976.

[23] Vincenzo Barone, Maurizio Casarin, Daniel Forrer, Michele Pavone, Mauro Sambi, and Andrea Vittadini. Role and effective treatment of dispersive forces in materials: Polyethylene and graphite crystals as test cases. *Journal of Computational Chemistry*, 30(6):934–939, 2009.

[24] Stefan Grimme. Semiempirical gga-type density functional constructed with a long-range dispersion correction. *Journal of Computational Chemistry*, 27(15):1787–1799, 2006.

[25] Nicola Marzari, David Vanderbilt, Alessandro De Vita, and M. C. Payne. Thermal contraction and disordering of the Al(110) surface. *Phys. Rev. Lett.*, 82:3296–3299, Apr 1999.

[26] Thomas A. Manz and Nidia Gabaldon Limas. Introducing DDEC6 atomic population analysis: part 1. charge partitioning theory and methodology. *RSC Adv.*, 6:47771–47801, 2016.

[27] Nidia Gabaldon Limas and Thomas A. Manz. Introducing DDEC6 atomic population analysis: part 2. computed results for a wide range of periodic and nonperiodic materials. *RSC Adv.*, 6:45727–45747, 2016.

[28] Zh. A. Boeva and V. G. Sergeyev. Polyaniline: Synthesis, properties, and application. *Polymer Science Series C*, 56(1):144–153, Sep 2014.

[29] J. S. Yoo, R. Christensen, T. Vegge, J. K. Norskov, and F. Studt. Theoretical insight into the trends that guide the electrochemical reduction of carbon dioxide to formic acid. *ChemSusChem*, 9:358, 2016.

[30] M. T. M. Koper. Thermodynamic theory of multi-electron transfer reactions: Implications for electrocatalysis. *J. Electroanal. Chem.*, 660:254, 2011.

[31] Javed Hussain, Hannes Jonsson, and Egill Skulason. Faraday efficiency and mechanism of electrochemical surface reactions: carbon dioxide reduction and H2 formation on Pt(111). *Faraday Discuss.*, 195:619–636, 2016.

[32] Suzanne Sirois, Miguel Castro, and Dennis R. Salahub. A density functional study of the interaction of CO2 with a Pd atom. *International Journal of Quantum Chemistry*, 52(S28):645–654, 1994.